Title
Investigating regional amyloid accumulation and cerebral blood flow reductions in aging and Alzheimer's disease

Author
LaPoint, Molly Rose

Publication Date
2023

Peer reviewed|Thesis/dissertation

Investigating regional amyloid accumulation and cerebral blood flow reductions in aging and Alzheimer's disease

By

Molly Rose LaPoint

A dissertation submitted in partial satisfaction of the

requirements for the degree of

Doctor of Philosophy

in

Neuroscience

in the

Graduate Division

of the

University of California, Berkeley

Committee in charge:

Professor William Jagust, Chair
Professor Silvia Bunge
Professor Chunlei Liu
Professor Kevin Weiner

Spring 2023

Abstract

Investigating regional amyloid accumulation and cerebral blood flow reductions in aging and Alzheimer's disease

By

Molly Rose LaPoint

Doctor of Philosophy in Neuroscience

University of California, Berkeley

Professor William Jagust, Chair

Alzheimer's disease (AD) is a form of dementia characterized by a long preclinical phase during which amyloid (Aβ) and tau proteins aggregate into plaques and tangles, respectively. The prevailing hypothesis holds that Aβ aggregation sets off a series of events, including tau aggregation and neurodegeneration, which ultimately leads to cognitive decline. Study of Aβ and tau aggregation has been facilitated in recent years by advances in positron emission tomography (PET), which allow serial imaging to understand what early factors affect clinical outcomes and progression to AD. Through this work, we know that older adults with high Aβ have greater levels of neurodegeneration and are at higher risk for developing AD. However, Aβ may be at its most toxic before it aggregates into insoluble plaques. This may mean that by the time global thresholds for Aβ positivity are reached, soluble forms of Aβ may have already begun the AD pathological cascade. As such, it is important to identify early levels of abnormal Aβ before cognitive decline and, to the extent that it is possible, before Aβ pathology is high everywhere.

The first project focuses on identifying early regions of Aβ deposition in cognitively normal older adults through PET imaging and creating a time course of regional Aβ burden. We found that parietal and frontal regions exhibited slightly earlier Aβ pathology than other studied regions, but that they all reached their peak accumulation rates within an eight-year span. Aβ accumulation in all brain regions studied was also similarly associated with apolipoprotein ε4 allele, a genetic risk factor for sporadic AD, and tau pathology. These results indicate that spread from one region to another is unlikely.

Neurodegeneration is widely thought to occur later in AD than Aβ and tau aggregation and can be studied with both PET and MRI measures. These measures do not always concur, so it can be useful to have both measures available. However, the main PET measure of neurodegeneration, [^{18}F] Fluorodeoxyglucose (FDG), which measures glucose metabolism, has been discontinued in many research studies because it adds an additional scan and radiation exposure. Thus, the second project investigates the use of relative delivery (R1), a proxy of cerebral blood flow derived from dynamic PET scans (which are often collected in research protocols), as an alternative measure to FDG. We found that R1 and FDG were highly correlated with one another and with MRI-based neurodegeneration measures. They were also similarly

associated with cognition in AD patients. This confirms that R1 can be used instead of FDG in situations where the latter is unavailable and may be particularly useful when dynamic PET scans are already being acquired.

Although cerebral blood flow is a proxy for neurodegeneration, it also reflects vascular function. A major question is whether vascular dysfunction leads to Aβ and tau accumulation, or whether changes in cerebral blood flow simply reflect neurodegeneration. Longitudinal investigations of Aβ, tau, and cerebral blood flow can help answer this question. The third project investigates change in R1 related to baseline Aβ/tau, and vice versa. We found that baseline Aβ predicted change in R1, but the opposite was not true, indicating that Aβ accumulation is upstream of cerebral blood flow and therefore it is less likely that blood flow changes drive amyloid deposition. Tau and R1 were correlated cross-sectionally and showed weak bidirectional longitudinal relationships that will require further study to untangle.

Taken together, these results further our understanding of the temporal dynamics of AD pathology and lend support to the Aβ cascade hypothesis. Our results indicate that the identification of a stable "early Aβ" region across studies with Aβ-PET is unlikely, and that cerebral blood flow measured with R1 is a proxy for neurodegeneration rather than reflecting early vascular pathology that incites AD.

Acknowledgements

First, I would like to thank Bill Jagust for his mentorship. The Jagust Lab has been a great place to work, full of very smart and kind people whose support has been instrumental to my research projects. I feel very lucky to have worked with you all. Special thank you to the research assistants, lab managers, and others who have conducted study visits over the years, collecting data to make my—and everyone else's—projects possible, and to the participants at Berkeley and UCSF who generously donated their time to be part of our studies.

I would especially like to thank Suzanne Baker, Susan Landau, and Tessa Harrison for their help with data processing, analysis, and manuscript revision on **Chapter 2.** I would like to thank Suzanne, Susan, and Alice Murphy for their help with **Chapter 3**; Renaud La Joie and Gil Rabinovici generously provided UCSF MAC data and assisted with the study, as well. For **Chapter 4**, I would again like to again thank all my previous coauthors, as well as Corrina Fonseca for providing me with some of the data used in my analyses. And, of course, thanks again go to Bill Jagust for the invaluable guidance and support with study design, interpretation, and revision for all my projects.

I am very grateful to my thesis committee, Silvia Bunge, Chunlei Liu, and Kevin Weiner, for their helpful suggestions and speedy review of my materials. The entire Helen Wills community has been a wonderful place to grow as a scientist. I'm thankful to my peers in the Neuroscience program, and my cohort especially, for being a fun and supportive group to learn alongside.

My former mentors at the Harvard Aging Brain Study and Boston College—especially Reisa Sperling, Aaron Schultz, Beth Mormino, and Sean MacEvoy—were instrumental in fostering my interest in neuroscience (and particularly aging/Alzheimer's disease) and getting me here to Berkeley. I feel especially lucky to have been part of the HABS team: my peers there are close friends with whom I've been navigating graduate school, and life, ever since. Thank you for being there.

Finally, thank you to all my friends near and far who have provided a listening ear during this chapter of my life. Special thank you to my parents and brother for being there from the beginning, and to my partner Will for supporting me and keeping me grounded these past few years.

Chapter 1: Introduction

β-amyloid plaques (Aβ) and neurofibrillary tangles (NFTs) composed of hyperphosphorylated tau are biological hallmarks of Alzheimer's disease (AD), a form of dementia characterized clinically by progressive cognitive decline. Research has shown about 30% of cognitively normal (CN) older adults display Aβ pathology in their brains, leading to the notion that there is a long preclinical phase to AD during which Aβ and tau are aggregating and neurodegeneration is occurring, but clinical symptoms have yet to appear (Braak and Braak, 1991; Sperling et al., 2011).

As the average lifespan increases, caring for those with dementia is an increasingly pressing concern, with estimates that 75 million individuals worldwide will be living with dementia in 2030, which will cost $2 trillion annually; there will be an estimated 132 million dementia patients in 2050 (Frankish and Horton, 2017). Thus, developing disease-modifying treatments for AD, the most common form of dementia, is of utmost importance. If we can characterize who is most likely to develop dementia during the preclinical phase of the disease, we may be able to identify disease-modifying targets that will allow dementia to be slowed, or even halted. Although AD can still only be definitively diagnosed at autopsy, the advent of radioligands to image AD pathology *in* vivo with positron emission tomography (PET) has been important to understanding the progression of the disease prior to symptom onset (Klunk et al., 2004; Schöll et al., 2016).

The amyloid cascade hypothesis posits that Aβ aggregation is the inciting event of AD (Jack et al., 2013a). Aβ accumulation appears to be necessary for tau aggregation into neurofibrillary tangles, temporoparietal neurodegeneration, and subsequent cognitive decline. Lending credence to this theory, Aducanamab, an anti-amyloid therapy, has been recently approved by the FDA for use in mild dementia, although there is concern that the clinical benefits are minor (Haddad et al., 2022). There is evidence that the most toxic form of Aβ is the soluble oligomers, which later aggregate into plaques, meaning that treatment occurring in symptomatic stages of the disease may be too late to see substantial clinical benefit (Haass and Selkoe, 2022). Thus, identifying abnormal Aβ levels as early as possible may provide immense benefit by targeting AD before serious neurodegeneration occurs. **Chapter 2** focuses on identifying potential early loci of Aβ accumulation that display elevated pathology before plaques appear diffusely throughout the brain.

In the amyloid cascade hypothesis framework, temporoparietal neurodegeneration follows Aβ accumulation. Temporoparietal neurodegeneration has been shown to continue after Aβ plateaus (Kadir et al., 2012; Nordberg et al., 2010). Neurodegeneration is more closely correlated with cognitive decline than with Aβ (Khosravi et al., 2019), and those who have both high Aβ and evidence of neurodegeneration fare worse cognitively than those with high Aβ alone (Hammond et al., 2020; Jack et al., 2018; Mormino et al., 2014). Thus, markers of Aβ and neurodegeneration provide complementary information about AD progression.

Neurodegeneration is assessed with both magnetic resonance imaging (MRI) and [^{18}F]-fluorodeoxyglucose (FDG), a PET radioligand that measures glucose metabolism. Although these measures are correlated, when dichotomized, MR measures and FDG only show weak agreement about who is neurodegeneration-positive (Jack et al., 2015). Some research studies have discontinued FDG scanning in in recent years due to the cost and participant burden associated with additional scanning time and radiation exposure, which makes studying

neurodegeneration effects more difficult. Methods exist, however, for extracting cerebral blood flow (CBF) information from dynamic PET scans. As CBF and glucose metabolism are tightly coupled (Bentourkia et al., 2000; Kuschinsky, 1991; Nihashi et al., 2007; Noda et al., 2002; Paulson et al., 2010), similar information may be captured by proxies of CBF derived from dynamic PET scans, which are often collected in the same research studies that have discontinued use of FDG. To validate this approach, **Chapter 3** compares FDG and PET-measured CBF, as well as MR-measured neurodegeneration, in a cohort of cognitively normal older adults and patients with AD and mild cognitive impairment (MCI).

Although a connection between neurodegeneration and CBF measures has been established, there is still debate as to what exactly CBF measures mean in the context of aging and AD, and when in the disease progression CBF changes occur. An alternative hypothesis to the amyloid cascade hypothesis is the vascular hypothesis of AD, which posits that vascular injury is the inciting event of AD. Under this theory, vascular risk factors or changes in cerebral blood flow drive oxidative stress, impair Aβ clearance from the brain, and promote the aggregation of Aβ and tau (de la Torre and Mussivan, 1993; Scheffer et al., 2021). If this hypothesis holds true, we expect that Aβ and tau aggregation would follow reductions in CBF. **Chapter 4** examines longitudinal change in CBF, Aβ, and tau pathology to investigate the temporal ordering of these pathological changes. **Chapter 5** will discuss how these three studies further our understanding of the timeline of AD pathology and the utility of PET biomarkers to identify early brain changes of the disease.

Mechanisms of Aβ and tau aggregation

Aβ is a cleavage product of the amyloid precursor protein (APP). APP is a transmembrane protein that under normal physiological conditions has been shown to facilitate neurite growth and promote cell adhesion (Thinakaran and Koo, 2008). APP may play an important role during embryonic development. APP knockout mice have lower cortical and hippocampal dendritic spine densities than wild-type mice, as well as impaired neuromuscular junction function and development. APP may promote long-term potentiation (LTP), a process through which synapses are strengthened over time and an important mechanism of learning and memory (Müller et al., 2017).

APP is cleaved at multiple sites intra- and extracellularly under normal physiological conditions. Cleavage by β and γ secretase creates Aβ peptides, which exist in multiple isoforms. The most common has 40 amino acids ($A\beta_{40}$), followed by the 42 amino acid form ($A\beta_{42}$). $A\beta_{42}$ is more prone to aggregation into plaques (Haass and Selkoe, 2007). Many forms of autosomal-dominant familial AD are caused by gene mutations promoting $A\beta_{42}$ cleavage over $A\beta_{40}$ (Thinakaran and Koo, 2008). The major known genetic risk factor for sporadic AD is the apolipoprotein E epsilon 4 (APOE ε4) allele; APOE is a lipoprotein transporter, and although its role in AD is not entirely understood, the ε4 allele is associated with aggregation and impaired clearance of Aβ (Kim et al., 2009). Aβ may be at its most toxic in soluble forms, before it aggregates into plaques. Soluble Aβ applied to rat hippocampal slices impairs LTP and reduces dendritic spine density; when applied *in vivo*, it disrupts memory performance. Insoluble plaques do not produce the same effect unless solubilized first (Shankar et al., 2008). In humans, postmortem levels of soluble Aβ levels better correlate with antemortem clinical measures (Näslund et al., 1999) and NFT density (McLean et al., 1999) than insoluble Aβ burden.

The tau protein has a physiological role in stabilization of microtubules and axonal transport. It becomes hyperphosphorylated in AD, which impairs its function by causing it to

detach from microtubules and ultimately aggregate into NFTs in the somatodendritic domain of neurons (Ittner and Götz, 2011). Although tau aggregation is seen in other neurodegenerative diseases, in AD its presence seems to be aggravated by Aβ. Injecting Aβ into the brains of aged rhesus monkeys leads to NFT formation and neurodegeneration (Geula et al., 1998) and transgenic mouse models of Aβ and tau aggregation show a marked acceleration of tau pathology compared to tau transgenic mice alone, whereas their Aβ levels are not increased (Götz et al., 2004; Pooler et al., 2015).

The temporal progression of tau pathology has been well-documented in both autopsy and PET studies, with NFTs beginning in the medial temporal lobe (MTL) and often seen in older adults without Aβ, spreading to inferolateral temporal cortex before becoming widespread throughout the brain, usually in the presence of Aβ (Braak and Braak, 1991; Schöll et al., 2016). The progression of Aβ plaques is less clear. Neuropathological studies have noted that there was variability in the location of plaques in early disease (Braak and Braak, 1991; Thal et al., 2002). PET studies in humans have also identified a variety of early regions, including frontal, temporal, and parietal cortex; consistent among these studies is that sensorimotor cortex and MTL regions are spared (Cho et al., 2016; Grothe et al., 2017; Guo et al., 2017; Jelistratova et al., 2020; Mattsson et al., 2019; Palmqvist et al., 2017; Villeneuve et al., 2015; Yotter et al., 2013). **Chapter 2** utilizes longitudinal Aβ-PET to examine early regions of plaque deposition.

PET imaging of AD-related brain changes

Although AD can only be diagnosed at autopsy, PET imaging has been a useful tool in both research and clinical settings. During a PET scan, subjects receive an intravenous injection of a radiopharmaceutical. The radiopharmaceutical is created using a cyclotron, which incorporates radioactive isotopes – typically ^{18}F or ^{11}C – into a biologically active molecule. PET scanners utilize a ring of sensors that detect paired gamma rays emitted by the radiotracer as it decays and can localize the origin of the positron-electron annihilation event because these paired gamma rays travel at an approximately 180-degree angle from one another.

To model PET scans, both differences in tissue absorption and tracer influx and efflux must be accounted for. CT or MRI scans are typically collected immediately prior to the PET scan for attenuation correction based on tissue absorption. PET data is typically collected once the initial influx of the tracer stabilizes. To account for individual differences and variability in the amount of tracer injected, subjects can undergo arterial sampling, which is invasive, or a ratio can be calculated of tracer amount in a region of interest (ROI) relative to a reference region, where binding of the tracer is low or not expected to change relative to a disease state. The standardized uptake value ratio (SUVR) is the ratio of tracer in the ROI relative to the reference region during this steady-state period of the scan.

One alternative to SUVR is distribution volume ratio (DVR), which can be used for reversibly-binding tracers and is a linear function of free receptor concentration in an ROI relative to a reference region (Logan et al., 1996). This typically involves placing the subject in the scanner at the time of tracer injection. To calculate signal, the simplified reference tissue model (SRTM) has three estimated variables: binding potential (BP), k'_2, the transfer of the tracer from the reference region to the plasma; and relative tracer delivery (R1), the transfer of the tracer to ROI tissue relative to reference region tissue (Lammertsma and Hume, 1996; Wu and Carson, 2002). This R1 measure can be used as a proxy of CBF as in **Chapters 3 and 4.**

Aβ PET tracers

Tracers for Aβ have been in use for nearly two decades, most notably[^{11}C] Pittsburgh Compound B (PIB) and [^{18}F] Florbetapir (Klunk et al., 2004). These tracers have shown that CN older adults with high levels of Aβ have worse cognition cross-sectionally (Rentz et al., 2010) and longitudinally (Landau et al., 2012), faster rates of brain atrophy (Chetelat et al., 2012) and a higher risk of progression to dementia (van der Kall et al., 2021). Studies often use cut points applied to global cortical ROIs to dichotomize their samples into Aβ-positive and -negative groups, which may not be as sensitive to the earliest increases in Aβ pathology. However, studies identifying early regions of Aβ pathology with PET imaging have found different results with respect to which regions exhibit the earliest pathological burden (Cho et al., 2016; Grothe et al., 2017; Guo et al., 2017; Mattsson et al., 2019; Palmqvist et al., 2017; Yotter et al., 2013). Given that Aβ may be most toxic before widespread plaque aggregation, reliable identification of focal elevated Aβ, before it reaches a global threshold of positivity, could have important implications for clinical trials.

The relationship between baseline and rate of change of Aβ-PET is quadratic, with rates of accumulation lower at high and low levels of baseline Aβ burden, and fastest in those with intermediate levels (Blautzik et al., 2017; Jack et al., 2013b; Jagust and Landau, 2021; Leal et al., 2018; Villemagne et al., 2013). From the quadratic function, a sigmoidal relationship between Aβ and time can be modeled. Though this has typically been applied to global Aβ-PET data, **Chapter 2** uses this method to place peak accumulation rates of regional Aβ along the time course of global Aβ accumulation in order to establish the time course of Aβ deposition in different regions relative to one another.

Tau PET tracers

Tracers for tau pathology are a newer development and include [^{18}F] flortaucipir (FTP), [^{18}F] THK derivatives, [^{11}C] PBB3, and [^{18}F] MK6240. Though these tracers have a high affinity for tau, their affinity for different tau isoform deposits varies, and some tracers exhibit high off-target binding (Okamura et al., 2018). Because of the off-target binding, partial volume correction methods are typically used to adjust for signal from one region, or from outside the brain, bleeding into an ROI or voxel of interest (Rousset et al., 1998). The topology of tau-PET closely mirrors autopsy studies, with tau spreading from the MTL (Johnson et al., 2016; Schöll et al., 2016; Vogel et al., 2020). Tau pathology is associated with atrophy and hypometabolism (LaPoint et al., 2017; Ossenkoppele et al., 2016) and individuals who have both elevated Aβ and elevated tau are most susceptible to cognitive decline (Pascoal et al., 2017). Regional Aβ and tau pathology are associated cross-sectionally in CN older adults (Lockhart et al., 2017), and **Chapter 2** demonstrates that regional Aβ accumulation is associated with temporal and parietal tau. **Chapter 4** follows up on analyses of MRI-based atrophy and hypometabolism, showing a longitudinal relationship between CBF—a measure of neurodegeneration—and tau-PET.

Imaging of glucose metabolism and CBF in AD

[^{18}F]-FDG-PET measures glucose metabolism and is used both in research and clinically to identify multiple diseases (Nordberg et al., 2010). AD patients exhibit a pattern of temporoparietal hypometabolism that correlates with disease severity and which can be useful in differential diagnosis (Jagust et al., 2007; Mosconi, 2005; Rabinovici et al., 2011). Hypometabolism also predicts cognitive decline in CN older adults (de Leon et al., 2001) and is associated with tau pathology (Ossenkoppele et al., 2016). Glucose metabolism and CBF are tightly coupled (Bentourkia et al., 2000; Kuschinsky, 1991; Nihashi et al., 2007; Noda et al.,

2002; Paulson et al., 2010), which has led many to view CBF measures as markers of neurodegeneration. Others, however, are proponents of the vascular hypothesis of AD and believe CBF may instead represent early vascular changes that are an inciting event of AD (de Leon et al., 2001; Scheffer et al., 2021). R1, a measure of PET tracer delivery to an ROI relative to a reference region, is a proxy of CBF used in **Chapters 3 and 4**. R1 specifically has been shown to correlate highly with FDG in older adults and AD patients (Meyer et al., 2011; Oliveira et al., 2018; Peretti et al., 2019; Rodriguez-Vieitez et al., 2017). **Chapter 3** confirms the correlation between R1 and FDG in a dataset of CN older adults and AD patients, and further shows that the two variables are similarly correlated with MRI-based measures of neurodegeneration and clinical severity. Little research has been done with longitudinal R1, but one study shows high test-retest reliability of R1, higher even than [^{15}O] H_2O-PET, often considered a gold standard of CBF measures (Bilgel et al., 2020). Longitudinal evaluation of R1 in concert with Aβ and tau measures in CN older adults could help establish whether CBF exhibits an early change consistent with the vascular hypothesis of AD—i.e., if baseline CBF predicts change in Aβ and tau pathology—or if it exhibits later changes consistent with neurodegeneration—i.e., baseline Aβ predicts CBF changes. A recent study found evidence of Aβ-R1 relationships in both directions, which could indicate R1 demonstrates both vascular and neurodegenerative changes (Ebenau et al., 2023). Our findings in **Chapter 4** indicate that baseline Aβ predicts change in R1, but not the reverse, confirming that R1-measured CBF exhibits later change consistent with a neurodegeneration marker. This chapter also examines R1-tau-PET relationships, which show cross-sectional correlations and weak bidirectional longitudinal associations that will require follow-up studies to further tease apart.

Chapter 2: Rates of β-amyloid deposition indicate widespread simultaneous accumulation throughout the brain

*This chapter is based on the following publication:
LaPoint, M.L., Baker, S.L., Landau, S.M., Harrison, T.M., Jagust, W. J. (2021). Rates of β-amyloid deposition indicate widespread simultaneous accumulation throughout the brain. *Neurobiology of Aging* 115: 1-11.

Abstract

Amyloid plaque aggregation is a pathological hallmark of Alzheimer's disease (AD) that occurs early in the disease. However, little is known about its progression throughout the brain. Using Pittsburgh Compound B (PIB)-PET imaging, we investigated the progression of regional amyloid accumulation in cognitively normal older adults. We found that all examined regions reached their peak accumulation rates 24-28 years after an estimated initiation corresponding to the mean baseline PIB-PET signal in amyloid-negative older adults. We also investigated the effect of increased genetic risk conferred by the apolipoprotein-E ε4 allele on rates of amyloid accumulation, as well as the relationship between regional amyloid accumulation and regional tau pathology, another hallmark of AD, measured with Flortaucipir-PET. Carriers of the ε4 allele had faster amyloid accumulation in all brain regions. Furthermore, in all regions excluding the temporal lobe, faster amyloid accumulation was associated with greater tau burden. These results indicate that amyloid accumulates near-simultaneously throughout the brain and is associated with higher AD pathology, and that genetic risk of AD is associated with faster amyloid accumulation.

Introduction

Amyloid-beta (Aβ) plaques are a hallmark of Alzheimer's disease and are also present in cognitively normal older adults. By their 70s, almost a third of older adults without cognitive impairment have extensive amyloid accumulation (Jack et al., 2008; Sperling et al., 2011). Cognitively unimpaired individuals with abnormal levels of Aβ may have subtle brain and cognitive changes consistent with the presence of a "preclinical" phase of Alzheimer's disease (AD) (Sperling et al., 2011). Thus, identifying the earliest stages of Aβ accumulation may be key to detecting who is at the highest risk for developing AD so that they can be followed closely, identified for clinical trials, and, if treatments become available, receive them in a timely manner.

Aβ can be measured *in vivo* using cerebrospinal fluid (CSF) and positron emission tomography (PET) with Aβ-sensitive radioligands. Often, studies assign participants to a "normal" or "abnormal" Aβ group based on cut points using CSF or a global PET measure which encompasses frontal, temporal, parietal, and cingulate cortices. This may be missing early stages of Aβ deposition when plaques may be present in only a subset of regions. Some studies have investigated the temporal progression of Aβ pathology, but the results have been inconsistent. Neuropathological studies typically show that association cortex deposition precedes medial temporal lobe (MTL), primary sensorimotor cortex, and subcortical areas (Braak and Braak, 1991; Thal et al., 2002), but the cortical regions shown to incur the earliest Aβ pathological burden with neuroimaging vary in both cross-sectional (Cho et al., 2016; Grothe et al., 2017; Villeneuve et al., 2015; Yotter et al., 2013) and existing longitudinal studies (Guo et al., 2017; Jelistratova et al., 2020; Mattsson et al., 2019; Palmqvist et al., 2017).

The goal of this study was to use cross-sectional and longitudinal Aβ-PET data to examine the regional changes in amyloid deposition when individuals are still cognitively normal. First, we replicated a method used previously (Cho et al., 2016) to show regions where elevated amyloid was seen cross-sectionally. The methods used in this paper for longitudinal analyses allowed us to investigate the time course of accumulation for each region, in addition to creating a sequential list of which regions appear to accumulate faster. For our cross-sectional analyses, we predicted that frontal, parietal, and lateral temporal regions would precede occipital, MTL, and sensorimotor regions. Identifying the earliest regions to display elevated Aβ might allow us to detect cognitively normal individuals who are at high risk for AD when measures of whole-brain Aβ burden are still below the threshold for positivity. This may also reveal potential mechanisms underlying the spread of Aβ. For example, if amyloid deposits appear in one region years before depositing in functionally-connected regions, this may indicate spread occurs through functional networks. On the other hand, if it appears in multiple regions at once, these regions may share certain tissue properties that affect their vulnerability to Aβ pathology (Whittington et al., 2018) . After regional amyloid accumulation is staged, the relationship between regional amyloid accumulation and risk factors for AD and other pathological markers of AD can be investigated.

One way to study longitudinal amyloid change is to examine the relationship between baseline Aβ burden and rate of change in Aβ burden, which is a quadratic function when measured globally (Blautzik et al., 2017; Jack et al., 2013b; Jagust and Landau, 2021; Villemagne et al., 2013). Using the quadratic equation representing this association, we can calculate a sigmoidal relationship between Aβ accumulation and time. The present study used this approach to investigate associations between regional slope and baseline global PET values to find the time course over which different regions reach their peak accumulation rates. The

results from these longitudinal analyses were compared to a previous cross-sectional staging method (Cho et al., 2016). Two previous studies have created a sigmoidal relationship between regional amyloid accumulation and time, one with modeled cross-sectional data (Whittington et al., 2018) and one with longitudinal data (Insel et al., 2020) and both show results inconsistent with long-term spread of Aβ from one region to another. We, however, predicted that frontal, parietal, and lateral temporal regions would reach their peak accumulation rate before occipital and MTL regions, but that most association cortex regions would show similar timing in Aβ accumulation.

In the process of examining rates of regional Ab accumulation, we also investigated the most important genetic factor involved in late onset AD, the Apolipoprotein E (*APOE*) genotype. Individuals with the ε4 allele are more likely to develop sporadic AD. In cognitively normal cohorts, ε4 carriers have been shown to have higher levels of Aβ pathology than noncarriers (Fouquet et al., 2014; Resnick et al., 2015). However, studies of longitudinal Aβ accumulation rates in ε4 carriers and noncarriers are inconsistent, with some finding no significant difference in accumulation rates and others showing higher accumulation rates in ε4 carriers than noncarriers(Burnham et al., 2020; Lim and Mormino, 2017; Mishra et al., 2018; Resnick et al., 2015). It is unclear if ε4 carriers simply develop Aβ earlier than noncarriers, but accumulate at the same rate, or if accumulation rate itself is faster in carriers versus noncarriers. Here we investigate the relationship between regional accumulation rates of Aβ in ε4 carriers and noncarriers, controlling for baseline levels of pathology in each region. We predicted that ε4 carriers would have faster accumulation rates in regions found to accumulate Aβ earlier (frontal, parietal, and lateral temporal regions) versus ε4 noncarriers.

Finally, we were interested in the association of Aβ accumulation with another pathological hallmark of AD, tau pathology. In contrast with Aβ, tau pathology accumulates following a stereotyped pattern beginning in the MTL (where high tau is common in older age), progressing to the surrounding inferolateral temporal lobes, and then spreading throughout the remaining cortex (Schöll et al., 2016; Vogel et al., 2020). Tau and Aβ burden are positively correlated in animal (He et al., 2018) and human studies (Lockhart et al., 2017; Vemuri et al., 2017) and individuals who have high levels of both are more likely to develop dementia (Pascoal et al., 2017).

The mechanisms by which high levels of tau and Aβ interact to create or contribute to cognitive decline are still unclear, especially since the regions susceptible to early tau and Aβ deposition do not overlap. While relationships between cross-sectional PET measures of Ab and tau have been explored (Lockhart et al., 2017), there are no data examining how the regional rates of Ab deposition may lead to regional tau deposition. Thus, we sought to investigate the relationship between Aβ accumulation rates and cross-sectional tau-PET proximate to the final Aβ measurement, within and between regions. By creating a map of early Aβ-depositing regions, we were able to investigate the relationships between regional accumulation rates and increased tau, both local and distant. We predicted that MTL tau would be associated with rates of Aβ accumulation in all regions, but that tau pathology outside the MTL would only be associated with accumulation in early Aβ regions.

Therefore, our study seeks to increase understanding of how the time course of Aβ accumulation varies by region, whether these accumulation rates differ in those with genetic risk for sporadic AD, and how accumulation rates in regions with different time courses associate with tau pathology in AD.

Materials and Methods

Participants

We recruited 195 participants from the Berkeley Aging Cohort Study (Mormino et al., 2009). All participants were cognitively normal, over 60 years of age, and had at least one [^{11}C] Pittsburgh compound B (PIB) Positron emission tomography (PET) scan for measurement of Aβ. A subset of 106 participants had more than one PIB-PET scan and were used for longitudinal analyses. Eighty-eight of these 106 participants had at least one [^{18}F] Flortaucipir (FTP) PET scan to measure tau pathology proximal to their final PIB-PET scan. All but 10 participants had FTP and PIB-PET scans on the same day and the median date difference was 0 days. Across all scans, the median difference between the PIB-PET and MRI scan was 8 days. Participant characteristics can be found in **Table 1.** Amyloid positive individuals were selectively recruited for longitudinal studies, producing an uncharacteristically high rate of amyloid positivity.

Sample	Cross-sectional	Longitudinal	FTP-PET
N	195	106	88
Female/Male	112/83	66/40	54/34
Age (years)	75.5 ± 5.97	75.0 ± 5.13	74.6 ± 4.93
Years of Education	16.9 ± 2.33	16.8 ± 1.86	17.0 ±2.54
Follow-up Time (years)	-	4.71 ± 3.07	4.91 ± 3.24
Number PIB scans (2,3,4,5)	-	52, 35, 13, 5	38, 32, 13, 5
PIB+/-	73/122	41/66	35/53
E4 carriers/noncarriers	45/134 (16 missing)	31/74 (1 missing)	25/62 (1 missing)

Table 1: Subject Demographics and descriptive statistics
A summary of all study participants. Participants in the longitudinal sample are a subset of the cross-sectional sample, and the FTP-PET sample is a further subset of the longitudinal sample.

Image Acquisition

[^{11}C] PIB was synthesized at Lawrence Berkeley National Lab (LBNL) Biomedical Isotope Facility as previously described (Mathis et al., 2003). PIB-PET imaging was carried out on one of two scanners, the ECAT EXACT HR or the BIOGRAPH PET/CT Truepoint 6. Previous studies have shown that there is no significant difference in distribution volume ratios (DVRs) between the two scanners (Elman et al., 2014a).

Details of PIB-PET scan acquisition have been previously outlined (Lockhart et al., 2017). Subjects received an intravenous injection of PIB (~15 mCi), at the beginning of 90 minutes of dynamic acquisition frames. The data were binned into 35 frames (4x15 seconds, 8x30 seconds, 9x60 seconds, 2x180 seconds, 10x300 seconds, and 2x600 seconds). A transmission or CT scan was acquired immediately before the emission scan for attenuation correction.

[^{18}F]FTP-PET was synthesized at LBNL based on a protocol provided by Avid Radiopharmaceuticals as previously described (Schöll et al., 2016). FTP scans were done on the BIOGRAPH scanner. Data acquired from 80-100 min post-injection were binned into 4x5 minute frames during reconstruction and used in subsequent analyses.

All PET images were reconstructed using an ordered subset expectation maximization algorithm with weighted attenuation, scatter correction, and smoothed with a 4mm Gaussian

kernel. Participants also underwent MRI on a 1.5 Tesla Siemens Magnetom Avanto MRI scanner at LBNL. A FreeSurfer (FS; http://surfer.nmr.mgh.harvard.edu/) version 5.3 segmentation of a T1-weighted magnetization prepared rapid gradient echo (MPRAGE) scan (TR/TE=2110/3.58 ms, FA=15°, 1x1×1 mm resolution) was used to parcellate PET scans into regions of interest (ROIs) for analysis of PET images.

Image Processing: PIB-PET

PIB-PET data were realigned, resliced, and coregistered to correspond to their closest structural scan from the 1.5 T MRI. There was a median of 7 days between the scans. Logan graphical analysis was used to calculate the DVR values as the slope of frames 35-90 minutes post-injection with a cerebellar reference region (Logan et al., 1996; Price et al., 2005). The structural MRI corresponding to each PET scan was processed with FS to derive ROIs in native space for each subject using the Desikan-Killiany atlas. The PET image was coregistered to the MRI, allowing us to calculate mean regional DVR values for each FS ROI. The global cortical PIB measure was calculated in native space for each participant (Mormino et al., 2011). In addition, the following FS regions were averaged to form larger composite cortical regions: lateral parietal (superior parietal, supramarginal, inferior parietal), medial parietal (precuneus, isthmus cingulate, posterior cingulate, paracentral), lateral frontal (rostral middle frontal, caudal middle frontal, pars orbitalis, pars triangularis, pars opercularis), medial frontal (superior frontal, caudal anterior cingulate, rostral anterior cingulate), orbitofrontal (OFC; frontal pole, medial and lateral orbitofrontal) sensorimotor (precentral and postcentral), inferior lateral temporal (fusiform, inferior and middle temporal), superior lateral temporal (superior temporal, transverse temporal, banks of the superior temporal sulcus), insula (insula), MTL (entorhinal and parahippocampal) and occipital (lateral occipital, lingual, cuneus, pericalcarine).

Image Processing: FTP-PET

FTP Standardized Uptake Value Ratio (SUVR) images were generated based on mean tracer uptake 80-100 minutes post-injection using an inferior cerebellar gray matter reference region (Baker et al., 2017). Like the PIB-PET data, the images were coregistered and resliced to each subject's 1.5 Tesla MR scan closest to the FTP scan. The scans occurred, on average, 30 days apart. SUVR images were partial volume corrected using the Geometric Transfer Matrix approach on FreeSurfer-derived values (Baker et al., 2017; Rousset et al., 1998). The same composite ROIs were calculated for FTP as for PIB.

Statistical Analyses

Statistical Analyses were conducted using MATLAB version 9.4 (R2018a; MathWorks, Inc., Natick, Massachusetts) and R version 3.4 (https://www.R- project.org/), including the packages *nlme* for analyses and *ggplot2* and *ggseg3d* for data visualization.

Statistical Analyses: Cross-sectional PIB staging analyses

We used cross-sectional data to infer a pattern of temporal progression of Aβ deposition, similar to methods used by others in staging Aβ pathology (Cho et al., 2016) in order to determine the ordering of positivity between regions, and to allow for comparison with the longitudinal methods. Mean and standard deviation values for each region were calculated in the subset of participants below the cutoff for PIB positivity (N = 122; DVR < 1.065)(Villeneuve et al., 2015). These values were used to Z-score each region's data for the entire sample. For each

region, the number of participants with a Z-score > 2.5 was counted and regions were ranked from those with the highest proportion of individuals with Z-scores > 2.5 to those with the lowest. Ties were broken by calculating the mean value of the Z-scores, with higher Z-score means leading to a higher ranking.

Statistical Analyses: Longitudinal PIB staging analyses

A linear function of DVR vs time was used to characterize the annual rate of change for subsequent analyses that minimized distance from a the regression line (Leal et al., 2018). Next, linear and quadratic models were fit in R using annual accumulation rate for each region (along with global PIB slope) and baseline global PIB values. In the linear model (slope ~ BL global PIB), regional slope was the dependent variable and global PIB was the independent variable. The quadratic model included the same parameters, but also included a baseline global PIB squared term (slope ~ BL global PIB + BL global PIB^2). For regions where both baseline global PIB terms were significantly associated with slope, Aikake Information Criterion (AIC) and residual sum of squares were used to compare the fit.

For regions where the quadratic model was a better fit, the maximum of the quadratic equation (created using the estimates from the model) could be found algebraically: for the function $f(x) = ax^2 + bx + c$, the maximum point is $(-b/(2a), f(-b/(2a))$. The x coordinate represents the global PIB DVR at which this region's PIB accumulation rate is fastest. Because all equations used baseline global PIB DVR as the independent variable, the global DVRs at which each region reaches its peak accumulation can be directly compared.

We next calculated the annual change in global DVR starting from the mean baseline global PIB DVR for PIB negative participants (DVR = 1.02). Annual change was calculated using the quadratic function through a time course of 50 years (Jagust and Landau, 2021). We also converted DVR values to Centiloids (CLs), a standardized scale allowing for comparison of Aβ accumulation using different Aβ-PET radiotracers (Klunk et al., 2015). Using CLs makes it easier to evaluate results between studies using not only different tracers, but also different processing methods for PIB. This approach enabled us to determine when accumulation in a region starts to decelerate, and understand how our results compare with those that have been done previously.

Statistical Analyses: PIB-APOE association

Participants were categorized as carriers or noncarriers of the APOE ε4 allele. Welch Two-Sample t-tests were used to compare PIB-PET slope between carriers and noncarriers. Because noncarrier longitudinal accumulation data did not fit quadratic models, linear models were used. Comparison of PIB-PET accumulation rates between groups used analysis of covariance (ANCOVA), controlling for baseline PIB-PET values, age, and sex.

Statistical Analyses: PIB-FTP association

Relationships between PIB-PET accumulation rates and FTP-PET within and across ROIs were examined using linear mixed effects models (LMEMs) carried out using the R package *nlme*. In these models FTP-PET was the dependent variable, with fixed effects PIB-PET, age, and sex as well as their interactions with time. The random effects were (1+time|subject), which modeled a subject-specific intercept and allowed the results to vary by subject over time. Again, local and distant analyses were run for all regions, as well as analyses examining the association between global PIB accumulation rate and regional tau. All statistics are reported at a liberal threshold of $p<0.05$, uncorrected.

Results

Cross-sectional results

The results of the cross-sectional analysis can be found in **Table 2**. There were small differences in the proportions of participants with abnormal values in frontal and parietal cortex. Regions with the lowest proportion of abnormal subjects were sensorimotor, MTL, and occipital.

Figure 1 shows these results graphically for each participant. Global PIB-PET captured the greatest number of people with elevated Aβ pathology. Furthermore, most participants were either above the cut points in all or nearly all regions or were not above the cut point in any region. Taken together with the finding that global PIB had the most participants above a Z-score of 2.5, this indicates that although some individuals show regionally specific PIB-PET signal, levels of PIB do not considerably differ by region.

Region	Percent Involvement	Z-score mean
Global PIB	26.7%	2.87
OFC	25.6%	2.16
Medial Parietal	25.1%	2.12
Medial Frontal	24.1%	2.16
Lateral Parietal	23.1%	1.85
Lateral Frontal	23.1%	2.43
Insula	23.1%	1.60
Inferior Lateral Temporal	22.1%	2.21
Superior Lateral Temporal	17.4%	1.59
Occipital	17.4%	1.01
MTL	16.9%	0.98
Sensorimotor	15.4%	1.08

Table 2: Z-Score Method Results
Cross-sectional analyses ranked regions based on the number of participants with elevated Aβ in each region. Elevated Aβ was defined as having a Z-score value above 2.5 standard deviations, based on the Aβ-negative participants.

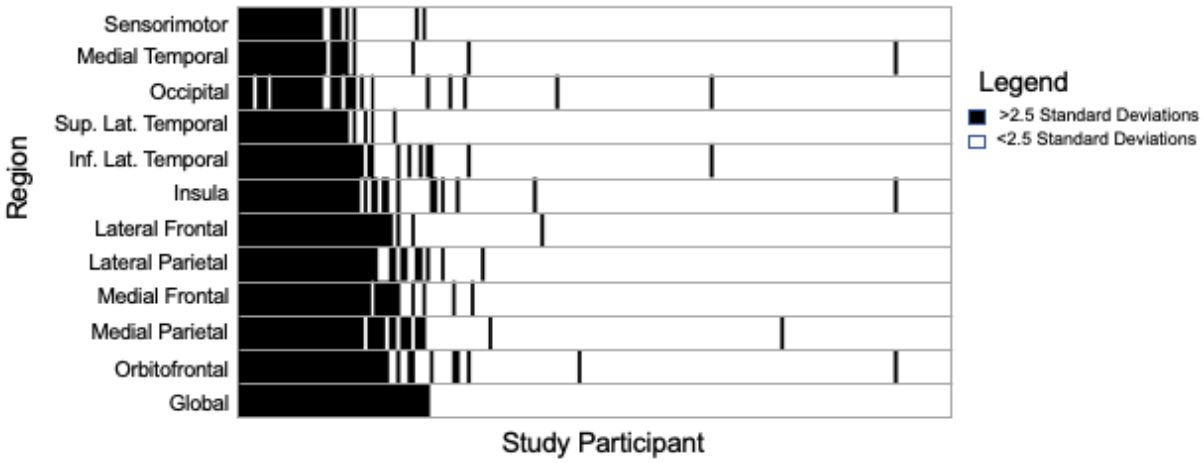

Figure 1: Regional PIB By Subject using Cross-Sectional Z-Score Method
In this figure, each participant is represented on the x-axis, in descending order by their global PIB DVR, and the regions are listed with on the y-axis. For each participant, the regions with a Z-score above 2.5 standard deviations are filled in black. Most participants who have elevated PIB-PET in one region have it in most or all other regions.

Longitudinal Results: Quadratic Model Fit

Quadratic models better fit the data in 8 of 11 regions and global PIB. The global PIB value at which each region reaches its fastest rate of accumulation, as well as the average rate of accumulation for each region, can be seen in **Table 3.** Neither the fastest accumulating (OFC; 0.014 DVR/year) or the slowest accumulating (MTL; 0.003 DVR/year) fit a quadratic. The first region to reach its peak accumulation rate was lateral parietal. Insula was the final one, with a difference in DVR of 0.13, CL value of 17, and an estimated time difference of 2-4 years. The quadratic fits for a subset of regions are plotted in **Figure 2.**

Region	*Global PIB DVR at peak regional slope*	*Mean slope (DVR/year)*	*Centiloid value at peak regional slope*	*Years to Peak Accumulation Rate*
Lateral Parietal	1.44	0.008	64	24-25
Sensorimotor	1.46	0.007	67	25-26
Medial Parietal	1.47	0.011	68	25-26
Medial Frontal	1.48	0.013	69	25-26
Lateral Frontal	1.48	0.010	69	25-26
Global PIB	1.50	0.011	73	26-27
Inferior Lateral Temporal	1.56	0.009	80	27-28
Superior Lateral Temporal	1.56	0.007	80	27-28
Insula	1.57	0.006	81	27-28

Table 3: Global PIB value at which each region reaches its peak accumulation rate
This table shows the global PIB DVR, Mean regional slope calculated with linear regression, Global PIB Centiloid value at peak, and number of years it takes for each region to reach its peak rate of accumulation using the quadratic fit. Parietal and frontal regions precede lateral temporal regions as well as the insula.

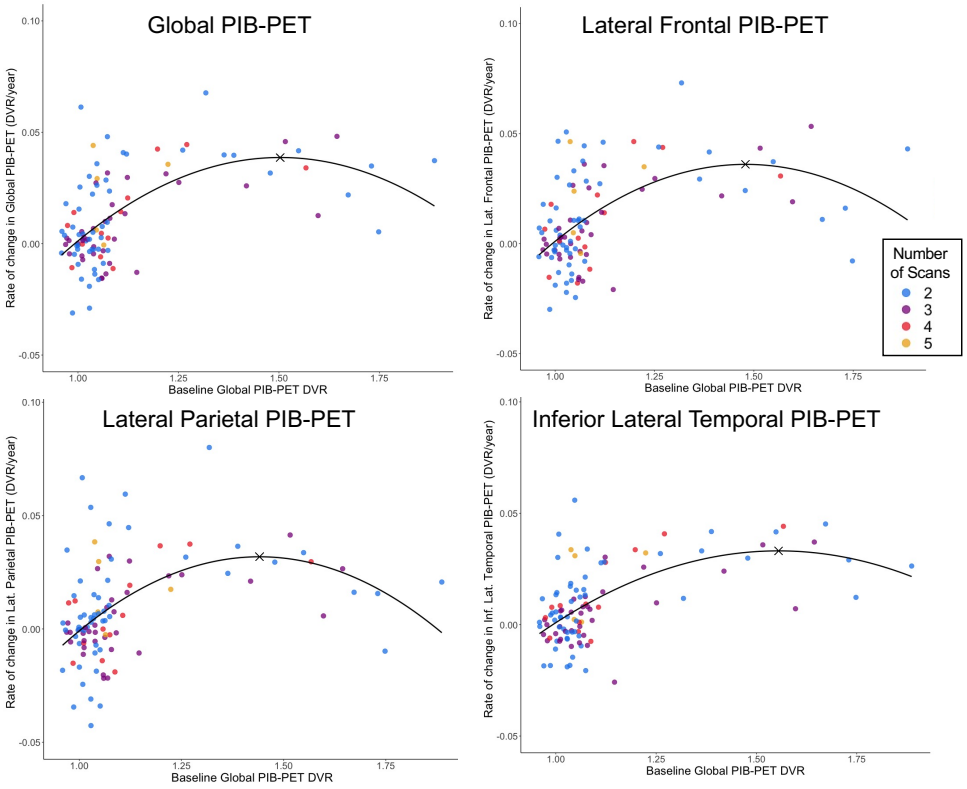

Figure 2: Quadratic Fit for a subset of regions
These figures show the relationships between global PIB at baseline and regional accumulation of amyloid for a subset of the analyzed regions. Global PIB is on the x-axis and regional change (DVR/year) is on the y-axis. Study participants are color coded according to how many PIB scans they have received. The black "X" on each graph is the point at which the regional slope is at its maximum. After this time point, regional PIB begins to decelerate.

Longitudinal Results: Regional PIB time course

Given a starting point of the mean global PIB value for PIB negative participants (DVR=1.02; CL=4), it would require 8-9 years to reach the threshold for PIB positivity (DVR=1.065; CL=10). The time course of global PIB accumulation can be seen in **Figure 3**, with the points at which select regions reach their peaks superimposed on the global PIB graph**.**

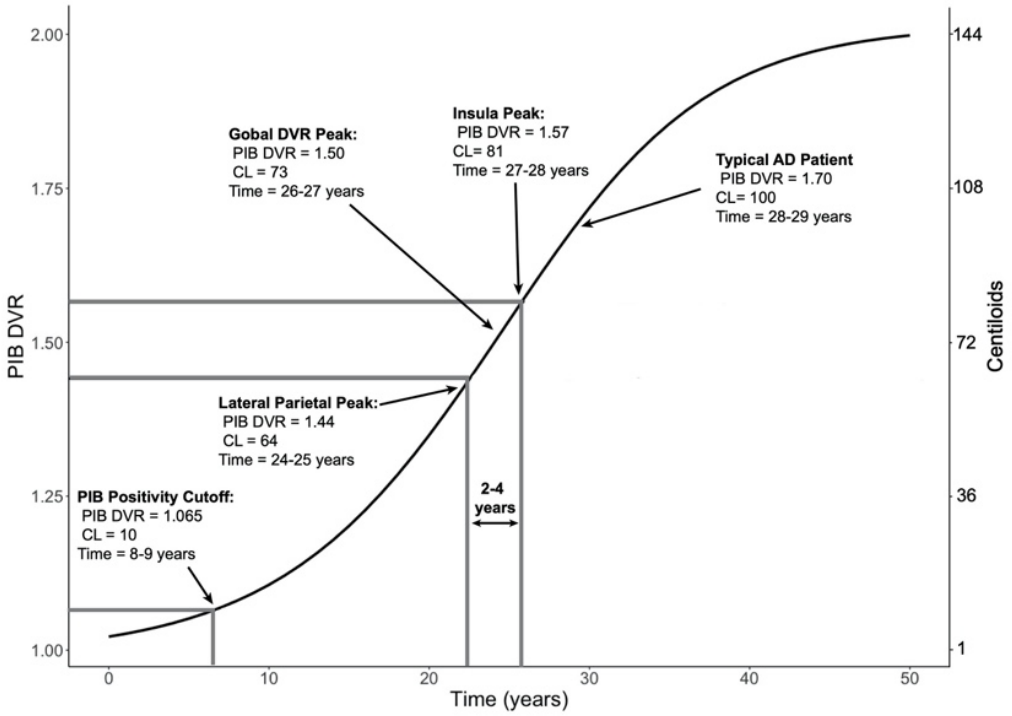

Figure 3: Sigmoidal time-global PIB relationship, showing different points of interest
This figure shows how global PIB DVR changes (y-axis) over 50 years, starting with the mean PIB DVR of amyloid-negative participants in the current study (DVR=1.02). It takes 8-9 years to reach a DVR of 1.065, the cutoff for PIB positivity in this sample, and the eight different regions reach their peak accumulation rates between 24 and 28 years from the mean baseline.

PIB-APOE relationships

In Welch two-sample t-tests, APOE ε4 carriers had higher baseline PIB values in all regions (linear models). In ANCOVA models, carriers had faster PIB accumulation rates in all regions, controlling for baseline PIB within that region, sex, and baseline age. A subset of associations between ε4 carrier status and regional slope are shown in **Figure 4.** The main effect of baseline was significant in all models except sensorimotor, occipital, and MTL, indicating that PIB accumulation is associated with *APOE* genotype above and beyond baseline PIB except in these later-accumulating regions.

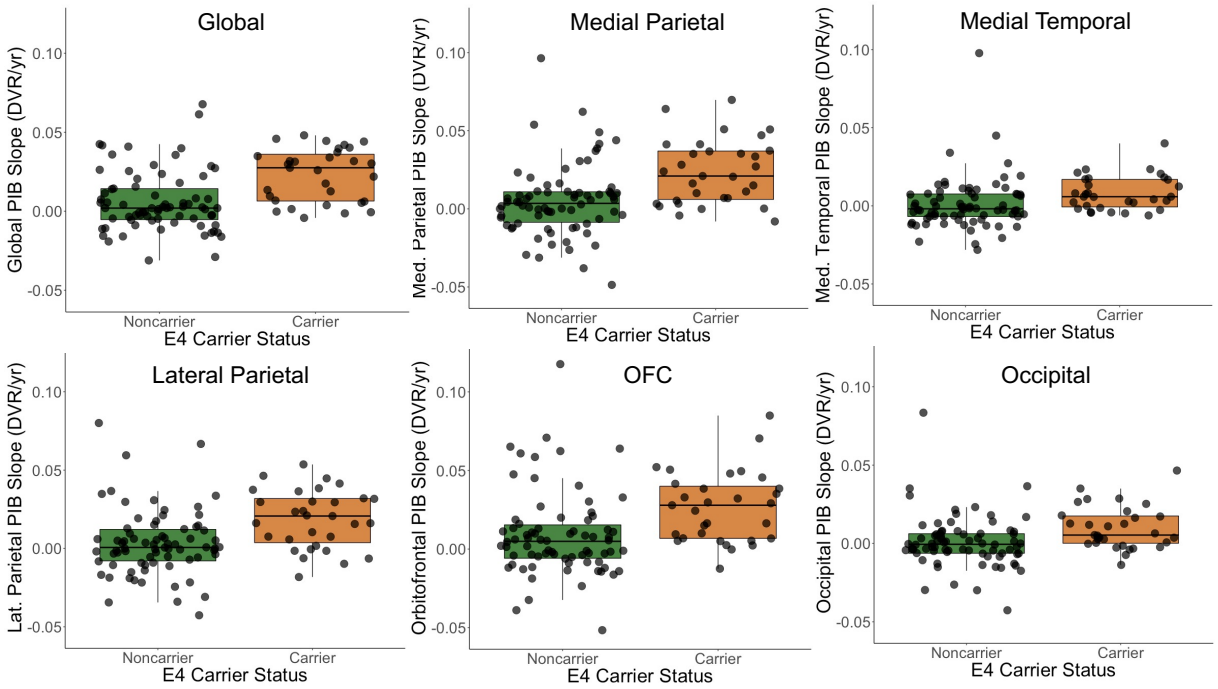

Figure 4: E4-PIB boxplots showing the accumulation rates in E4 carriers vs noncarriers
These plots show the rates of amyloid accumulation in ε4 noncarriers versus carriers. The relationships between regional accumulation and ε4 status are significant in all regions, controlling for baseline regional amyloid, sex, and baseline age, although this figure shows the uncorrected data. These boxplots. The bounds of the box show the 1st and 3rd quartile, and the middle line is the median. The whiskers indicate the minimum and maximum values within the bounds of the first quartile minus 1.5 multiplied by the interquartile range, or the third quartile plus the same value.

Tau-Aβ Relationships

Relationships between longitudinal PIB accumulation and FTP looked similar, regardless of the PIB region in LMEs **(Figure 5).** Local relationships were only seen between PIB accumulation rates and FTP in the lateral parietal ($t(157) = 2.28$, $p = 0.024$), superior lateral temporal ($t(157) = 2.19$, $p = 0.029$) and occipital regions ($t(157) = 2.70$, $p = 0.0078$). For most PIB regions, accumulation rate was most strongly associated with temporal FTP, especially lateral temporal regions, and lateral parietal FTP. PIB accumulation rates measured globally, and in medial parietal and OFC, were most strongly associated with FTP in temporoparietal brain regions, and also were associated with a wider distribution of FTP. Notably, these PIB regions, along with global PIB, were the four PIB measures with the highest percent involvement of PIB in cross-sectional methods and among the fastest accumulation rates.

Furthermore, PIB accumulation in the medial and inferior lateral temporal lobe was not associated with FTP in any region. Both regions had lower percent involvement of PIB in cross-sectional methods; inferior lateral temporal was one of the last regions to reach its peak accumulation rate in the quadratic analyses.

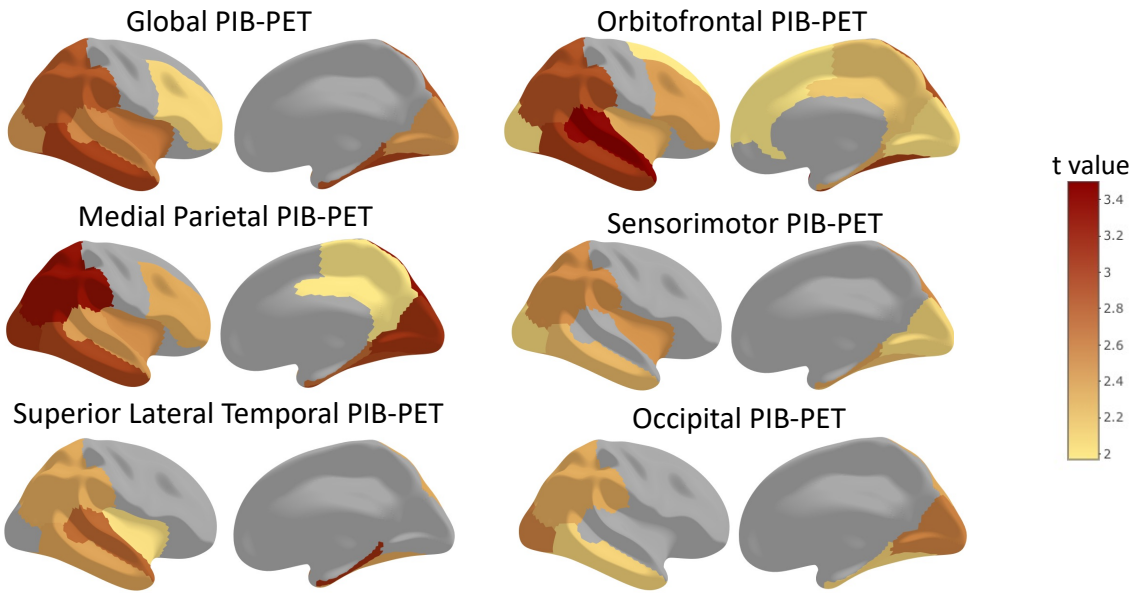

Figure 5: PIB-Tau relationships
Colors reflect the association between regional Aβ accumulation rates in the indicated brain region and regional FTP-PET at a liberal threshold of $p<0.05$, without correction for multiple comparisons. The pattern of associations between Aβ accumulation rates and tau deposition is similar across regions, with the strongest PIB-FTP relationships in temporal and lateral parietal regions and more moderate associations in global, OFC, and medial parietal PIB regions

Discussion

In this study, we investigated global rates of regional Aβ accumulation, and examined whether dynamics of Aβ accumulation in different brain regions differed from one another. This focus on both global and regional rates of Aβ accumulation allowed us to determine another measure of regional vulnerability to Aβ and permitted us to see how regional rates of Aβ accumulation related to APOE genotype and tau deposition. As anticipated, cross sectional results showed that global PIB-PET signal captured the most individuals with elevated Aβ. Those with high levels of PIB-PET in one region were likely to have high PIB-PET in most regions, but small differences between regions indicated that high levels of Aβ were most common in frontal and parietal regions, and least common in temporal cortex (particularly the MTL), the occipital lobe, and sensorimotor cortex. In longitudinal analyses, all investigated regions reach their peak accumulation rate within a span of four years (24-28 years after accumulation began), indicating that spread from one region to another is unlikely, or happens fast enough that no single region would be likely to have more utility in early diagnosis of AD than global measures of Aβ. Compared to noncarriers, APOE ε4 carriers had higher baseline Aβ and faster accumulation in all regions even after controlling for regional baseline Aβ. Lastly, faster Aβ accumulation was associated with elevated tau in temporal and parietal regions. These relationships were stronger and more widespread in the brain regions that deposited Aβ more rapidly, and no relationships were seen between Aβ accumulation in MTL or inferior lateral temporal regions and tau pathology in any region. Together, these results further our understanding of the regional dynamics of Aβ accumulation in unimpaired older adults and show how the rate of accumulation relates to genetics and tau pathology.

Regional Aβ Deposition

In the present study, there were regions that were more likely to harbor amyloid deposition than others, but most regions seemed to accumulate amyloid at a similar rate. Cross-sectionally, frontal and parietal regions were more likely to harbor elevated Aβ, and MTL sensorimotor, and occipital regions were less likely. Elevated Aβ in one region, however, was typically indicative of elevated Aβ throughout much of the cortex. These results are consistent with autopsy studies, in which frontal, parietal, and lateral temporal regions consistently show Aβ plaques before MTL and primary sensorimotor cortex (Braak and Braak, 1991; Thal et al., 2002). Cross-sectional Aβ-PET data show that deposition of Aβ in the sensorimotor cortex, occipital lobe, and medial temporal regions is less at early stages of AD (Cho et al., 2016; Grothe et al., 2017; Yotter et al., 2013). Our findings using the methods from Cho et al. (2016) largely replicate their results and add to a body of literature showing elevated Aβ in neocortical association areas with fewer individuals harboring high Aβ in MTL, sensorimotor, and occipital regions.

Cross-sectional results, however, do not address whether brain regions accumulate Aβ at different rates. In our longitudinal analyses, we found that all regions reached their peak accumulation rates 24-28 years after accumulation begins. A benefit of the present study is that, since accumulation in all regions was fitted to a quadratic with baseline global Aβ, we could directly compare the timing of accumulation. We found that, although some regions might accumulate Aβ slightly earlier or more quickly, the temporal differences between regional rates of Aβ accumulation are small. Many studies of regional Aβ have created staging schema using various methods. Some studies use cutoffs to identify regions that are elevated more often. One such study identified basal portions of the temporal lobe, the anterior cingulate, and parietal operculum as the earliest regions of deposition, with large portions of the frontal, parietal, and temporal lobes following in the second stage (Grothe et al., 2017). Although this staging method was created with cross-sectional data, it has been verified longitudinally (Jelistratova et al., 2020; Teipel et al., 2020). Others identify participants as Aβ accumulators or non-accumulators with the help of CSF measurements of Aβ, and compare where Aβ is highest, or where it is increasing fastest in accumulators versus non-accumulators. In these studies, earliest-stage Aβ appeared in the medial parietal lobe, medial frontal, and orbitofrontal cortex, with one additionally identifying lateral temporal regions (Mattsson et al., 2019; Palmqvist et al., 2017). Studies have also investigated either regions where participants have a high Aβ burden compared to their global Aβ value, or simply regions where either baseline Aβ burden is highest or where Aβ burden is increasing the fastest. Highest baseline values and fastest rates of change are often seen in the precuneus, anterior and posterior cingulate, and lateral frontal regions (Guo et al., 2018, 2017; Insel et al., 2020). What is typically consistent, however, is that medial temporal, occipital, and sensorimotor regions are among the final regions to become involved (Grothe et al., 2017; Guo et al., 2018, 2017; Mattsson et al., 2019; Palmqvist et al., 2017) Previous studies have often used clinically diverse cohorts including cognitively impaired participants. The wide array of regions that may define early stages of Aβ deposition may be due to demographic differences and/or PET radiotracer properties magnifying small differences in different cohorts.

This study is largely consistent with previous studies modeling the time course of Aβ over a sigmoidal trajectory. Important time points found in this paper and three others can be found in **Table 4.** Besides the present study, all other papers included cognitively impaired patients in their analyses (Jack et al., 2013b; Jagust and Landau, 2021; Villemagne et al., 2013). Despite these differences, the temporal patterns are surprisingly similar. From a starting point of

the mean Aβ burden of CNs, in the present study it would take 28-29 years to reach a typical Aβ burden for AD patients (equivalent to a CL value of 100), versus 28 years in ADNI (Jagust and Landau, 2021) and 31 years in AIBL (Villemagne et al., 2013). The time course in AIBL is very similar to the present study, with only the time to the Aβ positivity threshold more than approximately two years longer (12 years versus 8-9 years). In ADNI the starting point for the sigmoid is the same as the present study (4 CL) and the overall time course is very similar, but the amount of time it takes to reach the peak accumulation rate from the Aβ positivity threshold is much shorter (3 years versus 17-18 years) and the time to reach an average AD patient value from that peak is much longer (18 years versus 3-4 years). This may be due to the high number of cognitively impaired participants in the ADNI study (>60%) along with the requirement that only controls with positive amyloid-PET slopes were included. Data from the Mayo Clinic Study of Aging (MCSA) are somewhat difficult to compare because the starting SUVR for inclusion was higher. Perhaps for this reason, timing from a positive scan (an SUVR of 1.5) to a value typical of an AD patient required only about 14 years. Across all studies the most variable period of accumulation seems to be from the Aβ positivity threshold to the peak, which included values of 3, 6.6, and 18 years. Differences may be related in part to Aβ tracer used, or methodological differences in PET processing (such as the chosen reference region). This is a dynamic phase of Aβ accumulation and the inverted-U relationship is variable across studies, and any time course is relative to a study-defined starting point, so differences likely also reflect cohort composition.

Study	***This paper***	***ADNI (Jagust & Landau 2021)***	***MCSA (Jack et al. 2013)***	***AIBL (Villemagne et al. 2013)***
Sigmoid starting value	4 CL (AB- average)	4 CL (AB- average)	1.3 PIB SUVR	1.17 PIB SUVR (AB- average for accumulators)
Time from baseline to AB+ threshold	8-9 years 25 CL	7 years 25.3 CL	6.63 years (SUVR 1.5 to peak)	12 years
Time from AB+ threshold to peak	17-18 years	3 years	-	~17 years*
Time from peak to typical AD patient	3-4 years (94 CL)	18 years (100 CL)	7.66 years (peak to SUVR 2.5)	~2 years*

Table 4: Comparison of papers modeling the time course of amyloid accumulation
A comparison of four papers (the present study and three others) that have modeled the time course of amyloid accumulation in the Alzheimer's Disease Neuroimaging Initiative (ADNI), the Mayo Clinic Study of Aging (MCSA) and the Australian Imaging, Biomarkers and Lifestyle (AIBL) study. *Estimated from the papers' figures.

Two papers have modeled sigmoidal trajectories for regional Aβ (Insel et al., 2020; Whittington et al., 2018). Like in the present study, which modeled trajectories of regional accumulation relative to global Aβ so regional time courses can be compared on the same time scale, these results found limited differences in accumulation between regions. Insel and colleagues modeled accumulation of Aβ in different brain regions as a function of estimated disease time, and found that some regions, such as the precuneus and posterior cingulate, begin with high uptake and continue to increase in Aβ-PET uptake over time; other regions (lateral

OFC, isthmus cingulate, inferior parietal) start high but increase more slowly; in this report, all regions appear to reach their inflection point around the same time. This is similar to the findings of an earlier paper modeling accumulation with cross-sectional data, which concluded that amyloid accumulation begins simultaneously throughout the brain and that all regions reach their peak accumulation rates around the same time, with differences in the rate of accumulation based on carrying capacity (Whittington et al., 2018). This may help explain the somewhat surprising finding that sensorimotor cortex was one of the regions to reach its peak accumulation rate earlier despite relatively low levels of Aβ. This contrast between rapid accumulation rates and low values of Aβ may reflect two distinct processes, such that vulnerability may reflect either the rate of accumulation or the resulting amount of pathology.

Overall, these results indicate that significant inter-region spread of Aβ, through functional connections or otherwise, is not likely, given the short time differences between each region's peak accumulation rate. It seems more likely that regions which accumulate Aβ earlier share factors that make them vulnerable to aggregated Aβ peptide accumulation. They may, for example, have similar properties. In a study of regional gene expression, higher expression of the Aβ precursor protein (APP) gene, and reduced expression of genes involved in protein synthesis and mitochondrial respiration are associated with higher levels of Aβ-PET (Grothe et al., 2018). Patterns of regional metabolism are also implicated based on data showing that amyloid accumulating regions are involved in aerobic glycolysis (Vlassenko et al., 2010) and that they have lifelong elevated levels of glucose metabolism (Oh et al., 2016) These genetic and metabolic factors are likely to drive shared vulnerability resulting in Aβ aggregation appearing almost simultaneously in susceptible regions.

APOE-regional Aβ accumulation relationships

In this study, we also found that carriers of the APOE ε4 allele had faster accumulation of Aβ than noncarriers in all brain regions, adjusting for the difference in baseline Aβ. Our results are consistent with studies that report faster rates of accumulation in carriers (Burnham et al., 2020; Lim and Mormino, 2017; Mishra et al., 2018), although there are discrepancies (Lopresti et al., 2020; Resnick et al., 2015). Importantly, our data collected in cognitively normal individuals are congruent with literature reports that ε4 effects predominate in early phases of Aβ aggregation, and that after a certain point accumulation may no longer be faster (Burnham et al., 2020). Effects of this allele on Aβ deposition—particularly in shifting Aβ deposition earlier—are well known and indicate another factor that may be related to the similarity of accumulation rates throughout the brain.

Regional Aβ-tau relationships

Longitudinal associations between Aβ accumulation and tau mirrored the relationships found in our previous report with cross-sectional data (Lockhart et al., 2017) and were also similar to the pattern of elevated tau seen in studies investigating longitudinal global Aβ and tau (Tosun et al., 2017). Faster PIB accumulation in most regions was associated with cross-sectional FTP-PET in a relatively limited group of brain regions, with strongest relationships seen between PIB in multiple regions and FTP in the temporal lobe, where pathological tau is known to accumulate early in AD (Braak and Braak, 1991; Johnson et al., 2016; Schöll et al., 2016). Nevertheless, there were some regional associations between rates of Aβ accumulation and tau deposition, with no association between Aβ accumulation in inferior lateral and medial temporal lobes and tau pathology, and stronger associations between Aβ accumulation in faster

accumulating regions (OFC and medial parietal cortex) and tau pathology. The fact that regional Aβ accumulation was associated with a similar pattern of tau—especially temporal tau—is consistent with interpretations of prior cross-sectional data indicating that tau and Aβ pathology start in different regions, and that the location of Aβ accumulation bears non-specific relationship to the location of tau pathology both within and outside the temporal lobe. The similar findings for both cross-sectional and longitudinal Aβ accumulation raise crucial unanswered questions about how the widespread pattern of Aβ accumulation drives a relatively more focal deposition of tau pathology.

Limitations

There are some limitations to the present study. The sample size is relatively small, compared to some studies. About half the participants have only two PIB-PET time points, whereas it is optimal for longitudinal analyses to have three or more time points. In addition, all participants in the cohort are cognitively unimpaired. This is partially a strength and is helpful for characterizing early pathological changes and, as previously mentioned, verifying that Aβ accumulation in CN older adults follows a quadratic shape. However, it has drawbacks, such as limiting the number of high-Aβ ε4 noncarriers.

Aggregating the smaller, FreeSurfer-defined regions into larger regions is another potential limitation to the study. The data for small regions were noisy and did not typically follow a sigmoidal trajectory. Perhaps in a larger or more cognitively diverse cohort, sigmoidal functions could be fit for smaller regions. Similarly, the ideal way to compare ε4 carriers and noncarriers would be to fit separate quadratics. The noncarriers in this sample, however, did not fit a quadratic probably because of lower levels of Aβ in the noncarriers in particular. In a larger sample, or one with impaired individuals, there may be enough noncarriers with high accumulation rates, which would allow for the fitting of two separate quadratics. Finally, it is well known that Aβ-PET imaging is limited by the fact that it can only show us the location of Aβ plaques, which follow an earlier, oligomeric form of Aβ that is considered more toxic (Sakono and Zako, 2010; Salahuddin et al., 2016) is possible that the reason for inconsistencies in “early regions” or findings such as those in the present study that amyloid appears to arise near-simultaneously in many brain regions, is due to PET’s inability to image the very early phases of Aβ accumulation. However, there is currently no method to image oligomeric Aβ.

Conclusion

This study indicates that Aβ accumulates nearly simultaneously throughout the brain in cognitively normal older adults. Global Aβ accumulation follows a sigmoidal trajectory over time, and the time of peak accumulation of Aβ of different brain regions can be placed on that trajectory within a four-year span, peaking approximately 24-28 years after participants reach the mean baseline Aβ burden of cognitively normal, Aβ-negative older adults. Furthermore, faster rates of regional Aβ accumulation throughout the brain are associated with APOE ε4 allele carriage. Finally, faster accumulation of Aβ in nearly all regions was associated with elevated tau pathology, particularly in the temporal and parietal lobes. These results indicate that Aβ is unlikely to be spreading from one region to another, at least early in the disease process. In addition, this study shows that those who have faster rates of Aβ accumulation not only have elevated genetic risk for sporadic, late-onset AD, but also exhibit elevated burden of a second hallmark of AD, tau pathology.

Chapter 3: PIB-PET Relative delivery and FDG-PET are highly correlated and similarly associated with cognitive deficits in Alzheimer's Disease

*This chapter is based on the following manuscript:
LaPoint, M.L., Baker, S.L., Landau, S.M., Murphy, A., La Joie, R., Rabinovici, G.D., Jagust, W. J. PIB-PET Relative delivery and FDG-PET are highly correlated and similarly associated with cognitive deficits in Alzheimer's Disease. *In preparation.*

Abstract

Background

[^{18}F] Fluorodeoxyglucose PET (FDG) can measure neurodegeneration in Alzheimer's disease (AD) and aging. Because glucose metabolism and blood flow are coupled, PET measures of perfusion, such as relative delivery (R1), may capture similar information. This study compared FDG and R1 obtained from dynamic [^{11}C] Pittsburgh Compound B PET (PIB) in a sample of cognitively normal older adults (CNs) and amyloid-positive patients with mild cognitive impairment and mild dementia.

Methods

PIB and FDG-PET scans were acquired in 109 CNs and 84 patients within a one-year time frame. We compared their ability to discriminate amyloid-positive patients from CNs, investigated associations with MRI measures of neurodegeneration in all patients and a subset of CNs with 3 Tesla MR scans (N = 54), and compared associations between R1/FDG and performance on both the Clinical Dementia Rating and Mini Mental State Examination.

Results

R1 and FDG were both significantly lower in patients than in normal older adults and were able to discriminate between amyloid-negative controls and patients well, and with over 80% sensitivity and specificity. FDG and R1 also showed similar associations to cortical thickness in AD-vulnerable regions and hippocampal volume. In patients, R1 and FDG were associated with cognition in a similar set of regions, with lower R1/FDG predicting worse cognition.

Conclusion

These results indicate that R1 obtained from dynamic PIB scans is a useful indicator of neurodegeneration that may substitute for FDG in many studies.

Introduction

A hallmark of Alzheimer's disease (AD) is the β-amyloid (Aβ) plaque that can be imaged using a variety of PET ligands including [^{11}C] Pittsburgh Compound B (PIB) (Klunk et al., 2004). Neurodegeneration, reflected in brain atrophy or hypometabolism, can also be tracked with PET using [^{18}F]-fluorodeoxyglucose (FDG) (Minoshima et al., 1997; Nordberg et al., 2010; Rocher et al., 2003; Zimmer et al., 2017). Thus, FDG and PIB provide complementary information about disease. Glucose metabolism and cerebral blood flow (CBF) are tightly coupled (Nihashi et al., 2007; Paulson et al., 2010), and proxy measures of CBF can be calculated from dynamic PET scans. Relative tracer delivery (R1)—a ratio of the tracer influx from blood plasma to tissue in a region of interest (ROI) relative to a reference region—can be calculated from pharmacokinetic models such as the Simplified Reference Tissue Model (SRTM2) by collecting dynamic data immediately following tracer injection (Wu and Carson, 2002). In previous studies, R1 from PIB and other Aβ scans have been highly correlated with FDG and displayed similar patterns of uptake in both older adults and AD patients (Meyer et al., 2011; Oliveira et al., 2018; Peretti et al., 2019; Rodriguez-Vieitez et al., 2017). Existing studies, however, have not fully evaluated relationships between multiple measures of neurodegeneration and cognition that would place R1 on firm ground as a neurodegeneration biomarker.

The goal of this study is to compare R1 from dynamic PIB-PET scans and commonly used markers of neurodegeneration—both FDG-PET and MRI measures—in cognitively normal (CN) older adults and patients with dementia and mild cognitive impairment. First, we investigated the difference in R1 and FDG between CNs and patients. Next, we compared the associations between R1 and FDG, hippocampal volume, and cortical thickness in AD-vulnerable regions. Finally, we compared the associations across the cortex between R1 and cognition and FDG-PET and cognition. Overall, our hypotheses were that R1 measures would show findings similar to FDG: reduced perfusion in patients and ability to differentiate patients and controls and correlation with regional atrophy and cognition.

Materials and Methods

Study Participants

We recruited 109 CNs from the Berkeley Aging Cohort Study (BACS), an ongoing longitudinal study of cognitive aging (Mormino et al., 2009). An additional 84 participants with cognitive impairment came from the University of California, San Francisco Memory and Aging Center (UCSF MAC). Participants from the UCSF MAC underwent a standard dementia screening including a physical examination, evaluation of medical history, caregiver interview, MRI, and neuropsychological testing (Ossenkoppele et al., 2016). All participants or their surrogates gave written and informed consent. Studies were approved by the University of California San Francisco, University of California Berkeley, and Lawrence Berkeley National Laboratory institutional review boards for human research.

Clinical diagnosis was established by consensus in a multidisciplinary team and all patients fulfilled criteria for MCI or mild dementia and had positive PIB-PET scans (DVR ≥ 1.065). Many patients in this sample have early onset AD, often presenting with non-amnestic phenotypes (La Joie et al., 2021). All participants had a PIB and FDG scans within one year. All UCSF patients and a subset of BACS participants (N=53) had a 3T MRI scan.

PET Acquisition

[^{11}C] PIB was synthesized at Lawrence Berkeley National Lab (LBNL) Biomedical Isotope Facility as previously described (Mathis et al., 2003). Participants received an intravenous injection of PIB (~15 mCi) at the beginning of 90 minutes of dynamic frame acquisition. The data were binned into 35 frames (4x15 seconds, 8x30 seconds, 9x60 seconds, 2x180 seconds, 10x300 seconds, and 2x600 seconds). These methods have been previously described in more depth (Lockhart et al., 2017). FDG was provided by IBA Molecular and acquired in six emission frames of five minutes each, \30-60 minutes post-injection.

A transmission or CT scan was acquired immediately before all emission scans for attenuation correction. Data were collected on one of two scanners, the ECAT EXACT HR (N=64) or the BIOGRAPH PET/CT Truepoint 6 (N=129). Previous studies have shown no significant difference in PIB DVRs (Elman et al., 2014a). All PET images were reconstructed using an ordered subset expectation maximization algorithm with weighted attenuation, scatter correction, and smoothed with a 4mm Gaussian kernel.

MRI Acquisition and Processing

CN participants received two MRIs. A 1.5T scan at LBNL was performed on a Siemens Magnetom Avanto System which included collection of a T1-weighted magnetization prepared rapid gradient echo (MPRAGE) scan (TR/TE=2110/3.58 ms, FA=15°, 1x1×1 mm resolution) used for coregistration of PET scans and definition of ROIs for analysis.

3T MR imaging was performed in a subset of 53 CN participants at the Henry H. Wheeler Jr. Brain Imaging Center at University of California, Berkeley on a Siemens 3T TIM/Trio scanner with a 32-channel head coil. High-resolution whole brain structural images were acquired using a T1-weighted volumetric MPRAGE (voxel size = 1 mm isotropic, TR = 2300 ms, TE = 2.98 ms). These scans were analyzed for cortical thickness and hippocampal volume.

MRI acquisition for patients was performed at the UCSF Neuroscience Imaging Center on a 3T Siemens TIM/Trio (N=45) or Prisma (N=42) scanner with a 12-channel head coil. A T1-weighted MPRAGE was collected (For both, TR=2300 ms; TE=2.98 ms; inversion time, 900 ms; FA=9°; Prisma TE=2.9 ms and Trio TE=2.98 ms). These scans were used for coregistration/ROI definition and for measurement of cortical thickness and hippocampal volume.

FreeSurfer (FS, https://surfer.nmr.mgh.harvard.edu/) version 5.3 was used to process each MPRAGE to derive ROIs from the Desikan-Killiany atlas, along with FS version 7.0 brainstem segmentation. A pons ROI was used to define the reference region (Iglesias et al., 2015) and a FS-defined metaROI was used as the target region for FDG and R1, consisting of bilateral isthmus cingulate, middle temporal, and inferior parietal ROIs. FDG and R1 values were also calculated for each cortical FS ROI, as well as the hippocampus and amygdala.

Adjusted hippocampal volume was calculated by summing the left and right hippocampus ROIs from 3T scans, dividing by the intracranial volume, and multiplying by 1,000 for scaling. An “AD signature” ROI sensitive to neurodegeneration was created via a weighted average of entorhinal, fusiform, inferior temporal, and middle temporal thickness (Jack et al., 2015).

PET Processing

PIB-PET data were realigned, resliced, and coregistered to correspond to their closest structural scan from 1.5 T MRI (CNs) or 3T MRI (patients) using Statistical Parametric Mapping 12 (SPM12, https://www.fil.ion.ucl.ac.uk/spm/). Logan graphical analysis was used to calculate the DVR values as the slope of frames 35-90 minutes post-injection with a cerebellar reference

region (Logan et al., 1996; Price et al., 2005). A global cortical PIB DVR was calculated to define PIB status (Mormino et al., 2011).

Resliced and MRI-coregistered PET images were also used for R1 calculation. R1 values were derived using SRTM2 from full-scan time activity curves on a regional basis. The pons was used as the reference region. In SRMT2, a global reference region clearance constant is calculated for the reference region (k'_2) within each subject to reduce noise.

FDG-PET data were also realigned, averaged, resliced, and coregistered to the subject's MRI using SPM12. Standardized uptake value (SUV) images were calculated based on mean tracer uptake 30-60 minutes post-injection and normalized to a pons reference region to create an SUV ratio (SUVR) image. SUVR values were calculated for FS ROIs analysis.

Clinical Assessments

Global measures of cognition were examined in relation to FDG and R1 measurements. Mini Mental State Examination (MMSE) and the Clinical Dementia Rating Sum of Boxes (CDR-SB) were used to evaluate cognition of patients (Folstein et al., 1975; Morris, 1993). These data were collected within a year of the PIB scan.

Statistical Analyses

Statistical analyses were performed in R (version 4.0.2; https://www.R-project.org/) and MATLAB (version 9.7, R2019b; MathWorks, Inc., Natick, Massachusetts). R packages *ggplot2* and *ggseg* were used for visualizations (Mowinkel and Vidal-Piñeiro, 2019).

To determine differences in R1 and FDG between Aβ- CNs, Aβ+ CNs, and patients, we performed one-way repeated measures ANCOVAs with region (FDG or R1) as the within-subjects variable, subject group as the between-subjects variable, and age and sex as covariates. For these analyses, we investigated each of the metaROI's component regions. Following these analyses, we ran ANCOVAs for each region and the metaROI separately. We also examined correlations between FDG and R1 in the metaROI in the whole sample and between Aβ- CNs, Aβ+ CNs, and patients.

Next, we compared correlations between metaROI R1/FDG and MRI measures of neurodegeneration—hippocampal volume and AD signature thickness. We calculated the correlation coefficients for R1 and FDG and each measure of neurodegeneration. We also compared the ability of each measure to distinguish between Aβ- CNs and patients by fitting a logistic regression function to the data, with the measure of interest (R1, FDG, hippocampal volume, or AD signature thickness) as the independent variable and subject group as the dependent variable. To evaluate different thresholds, we plotted a receiver operating characteristic (ROC) curve using the R package *pROC*. These analyses were conducted in the FDG and R1 metaROI in the whole group and repeated with all four measures in the subset with 3T MRI. Youden's Index was used to determine the sensitivity and specificity of the optimum cut points (Youden, 1950).

The final analyses focused on comparing the relationships between FDG and R1 to clinical deficits in the patients. We used linear regression models, with MMSE or CDR-SB as the dependent variable, R1 and FDG values as the independent variable, and age and sex as covariates. All cortical FS ROIs, the metaROI, and hippocampus were analyzed. In addition, the Fisher *z*-transformation of the Pearson correlation coefficient between R1 and FDG and MMSE/CDR-SB for each ROI was calculated, so the analyses could be more directly compared. We calculated the correlation coefficient for the FDG-cognition transformed correlations and the

R1-cognition transformed correlations, to discern how similarly FDG and R1 performed in each analysis.

Results

Sample Characteristics

Subject demographics and descriptive statistics are shown in **Table 1**.
Patients were significantly younger than CNs ($t(134.18) = 9.23$, $p < 0.000001$). The patient sample includes a variety of clinical AD phenotypes. All patients were Aβ+. The CNs had more females than males, while the patient cohort was more balanced.

	Main Sample		**3T MRI Subsample**
	CNs N = 109	**Patients** N = 84	**CNs** N = 53
Aβ status (-/+)	68/41	0/84	27/26
Age	76.3 ± 6.3	64.2 ± 9.6	77.4 ± 6.5
Sex (F/M)	73/36	41/43	36/17
MMSE	28.9 ± 1.6	21.2 ± 2.2*	28.8 ± 1.9
CDR-SB	-	4.4 ± 2.2	-
Diagnosis	-	40 AD 16 PCA 11 lvPPA 17 MCI	-

Table 1: Participant demographics and descriptive statistics. Patients were significantly younger than cognitively normal (CN) participants. *One subject was missing MMSE score. Abbreviations: AD: Alzheimer's disease; PCA: posterior cortical atrophy; lvPPA: logopenic variant primary progressive aphasia; MCI: mild cognitive impairment.

R1 and FDG in CNs vs. Patients

In the repeated measures ANCOVA, there was a main effect of subject group for both FDG and R1 (FDG: $F(2,188) = 62.9$, $p < 0.001$; R1: $(2,188) = 52.6$, $p < 0.001$). For the individual models, there was a statistically significant difference between the three groups (Aβ+ CNs, Aβ- CNs, patients) in all regions for both R1 and FDG, with similar effect sizes as measured with partial $\eta 2$ (R1 metaROI: $F(2,188) = 69.5$, partial $\eta 2 = 0.316$; FDG metaROI: $F(2,188) = 90.9$, partial $\eta 2 = 0.356$). T-tests were used to assess differences between groups and found no significant differences between the Aβ- and Aβ+ CNs for any ROI. The CNs (collapsed across Aβ status) had significantly higher R1 and FDG values than the patients in every region **(Figure 1)**.The correlation between metaROI values for FDG and R1 was also significant, in both the whole sample ($t(191) = 17.53$, $p < 1E\text{-}6$, $r = 0.785$) and each subject group (Aβ-: CN $t(66) = 7.20$, $p < 1E\text{-}6$, , $r= 0.631$; Aβ+ CN: $t(39) = 3.81$, $p =0.0005$, $r= 0.521$; patients: : $t(82) = 7.70$, $p < 1E6$, $r= 0.648$; **Figure 1)**.

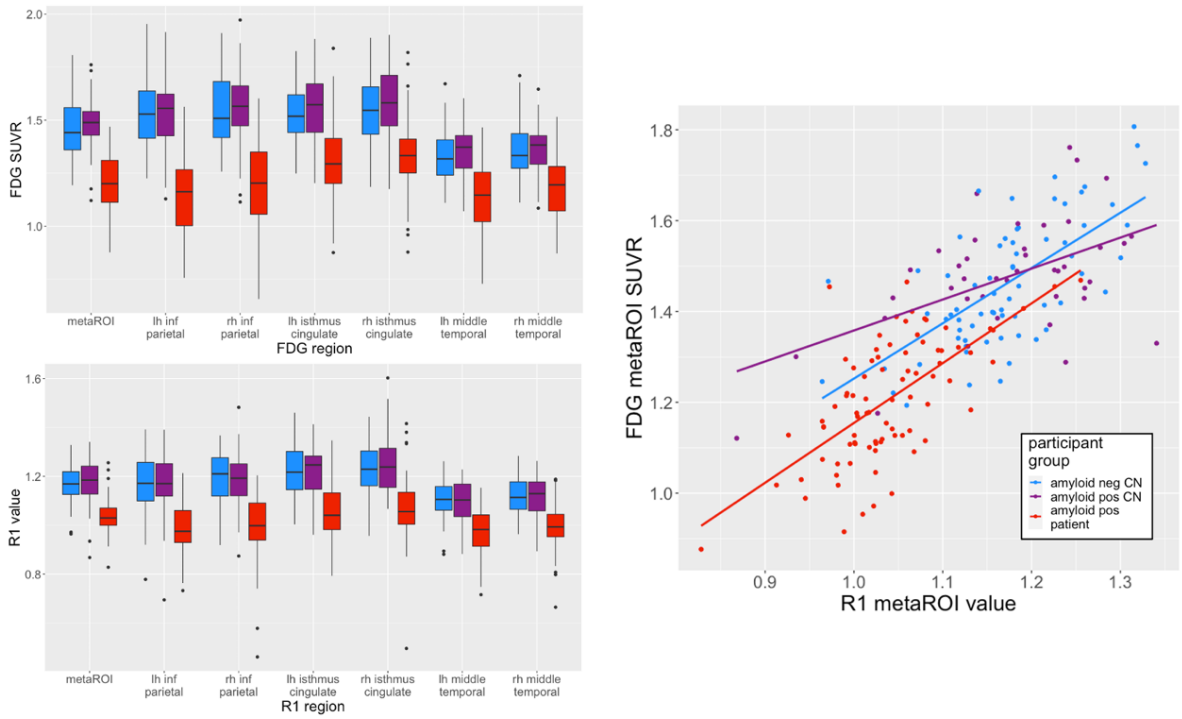

Figure 1: R1 and FDG was lower in patients than in cognitively normal participants (left). R1 and FDG in the metaROI were significantly correlated with one another (right). The analyses had similar effect sizes.

R1 and FDG vs MR measures of neurodegeneration

In the whole sample, AD signature thickness and hippocampal volume were positively correlated with both R1 (AD signature: $t(135) = 9.97$, $p<1E6$, $r = 0.566$; hippocampal volume: $t(135) = 4.13$, $p = 0.00006$, $r = 0.335$) and FDG (AD signature: $t(135) = 8.39$, $p<1E6$, $r = 0.586$); hippocampal volume: $t(135) = 3.57$, $p=0.0005$, $r = 0.294$).

The results, however, were driven by different groups. For hippocampal volume, the results were driven by the CN groups. In R1, the correlation was significant in both CN groups (Aβ-: $t(25) = 2.17$, $p = 0.04$, $r = 0.298$; Aβ+ CN: $t(24) = 2.59$, $p = 0.02$, $r = 0.227$; patient: $t=0.77$, $p > 0.5$, $r = 0.085$). In FDG, the correlation was significant only in the Aβ+ group (Aβ-: $t = 1.75$, $p = 0.08$, $r = 0.331$; Aβ+: $t = 3.30$, $p = 0.003$, $r = 0.559$; patient: $t = 0.19$, $p > 0.8$, $r = 0.021$).

For AD signature thickness, however, only the patients had a significant correlation with R1 (patients: $t(82) = 7.70$, $p < 1E-6$, $r = 0.508$; Aβ- CN: $t(25) = 0.8$, $p > 0.7$, $r = -0.158$; Aβ+ CN: $t(24) = 1.14$, $p > 02$, $r = 0.227$) and FDG (patients: $t(82) = 5.31$, $p < 1E-6$, $r = 0.506$; Aβ- CN: $t(25) = 0.66$, $p > 0.5$, $r = -0.131$; Aβ+ CN: $t(24) = 0.85$, $p > 0.2$, $r = 0.171$). The results of these analyses are depicted in **Figure 2**.

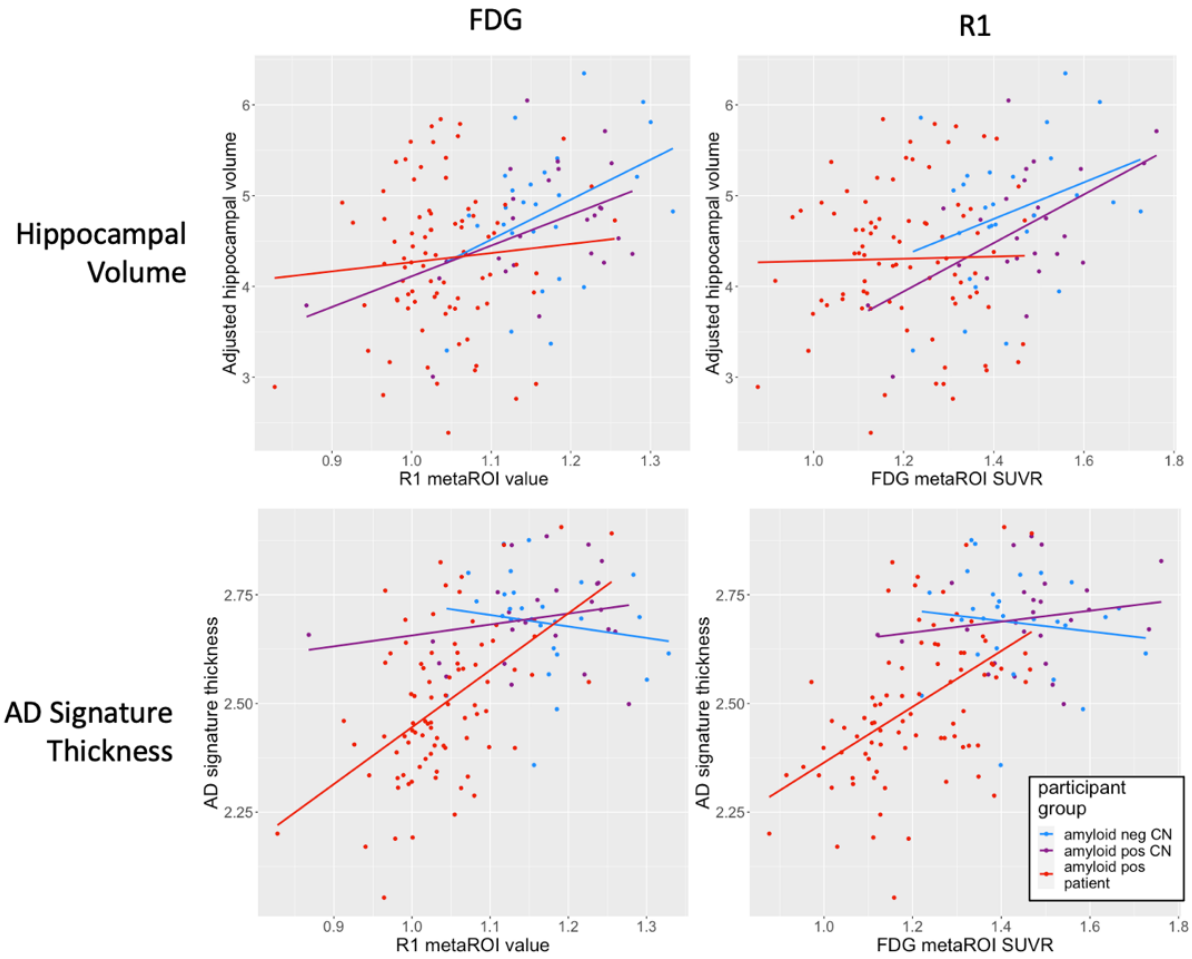

Figure 2: R1/FDG metaROI correlations with structural measures of neurodegeneration. FDG (left) and R1 (right) showed similar correlations with hippocampal volume adjusted for intracranial volume (top) and AD signature ROI thickness (bottom). AD signature thickness and hippocampal volume were positively correlated with both R1 and FDG. The R1/FDG relationship with hippocampal volume was driven by CNs, while the relationship with AD signature thickness was driven by the patients.

ROC Curve Analyses

ROC curves comparing the ability of each measure to distinguish between Aβ- controls and patients can be seen in **Figure 3.** For R1, AUC = 0.907 (95% CI 0.8567-0.9556) and for FDG, AUC = 0.908 (95% CI 0.8636-0.9516). The optimum threshold for R1 yielded a sensitivity and specificity of 0.88, while for the FDG threshold, specificity = 0.82 and sensitivity = 0.85. The results were similar for R1 and FDG in the MRI subsample (R1: sensitivity and specificity = 0.89; FDG: specificity = 0.80, sensitivity = 0.89). AD signature thickness performed slightly worse (specificity = 0.75, sensitivity = 0.81) and both measures for hippocampal volume were <80% (specificity = 0.61, sensitivity = 0.78).

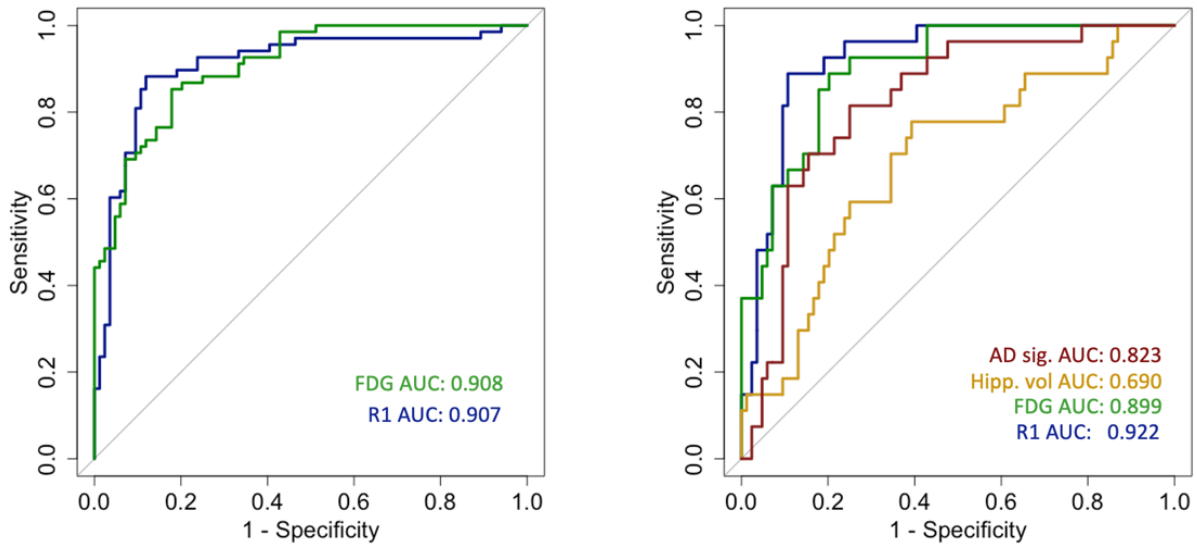

Figure 3: Receiver operating characteristic (ROC) curves comparing the ability of different neurodegeneration markers in their ability to discriminate amyloid-negative cognitively normal older adults from amyloid-positive patients via logistic regression. R1 and FDG metaROIs performed similarly in the whole sample. In the subsample with MR measures of neurodegeneration, R1 and FDG performed better than Alzheimer's disease signature ROI thickness and adjusted hippocampal volume.

R1/FDG-Cognition Analyses

In patients, R1 and FDG were associated with both cognitive measures in a similar pattern, although the relationships between FDG and MMSE/CDR-SB were more extensive. Significant associations were primarily seen in the lateral temporal and parietal lobes, cingulate cortex, and frontal lobe. The regions that show a significant association for each analysis are depicted in **Figure 4**. All regions with $p<0.05$ are shown without correction for multiple comparisons, as we were primarily interested in the pattern of relationships.

We found a high correlation between FDG-MMSE/CDR-SB and R1-MMSE/CDR-SB Fisher z-transformed correlations across brain regions **(Figure 5)**. These correlations were statistically significant (MMSE: $t(71) = 22.36$, $p < 1E\text{-}6$, $r = 0.936$; CDR-SB: $t(71) = 12.04$, $p < 1E\text{-}6$, $r = 0.819$). Each point on the figure represents the correlation between FDG-cognition Fisher z-transformed value and the R1-cognition z-transformed value in one brain region.

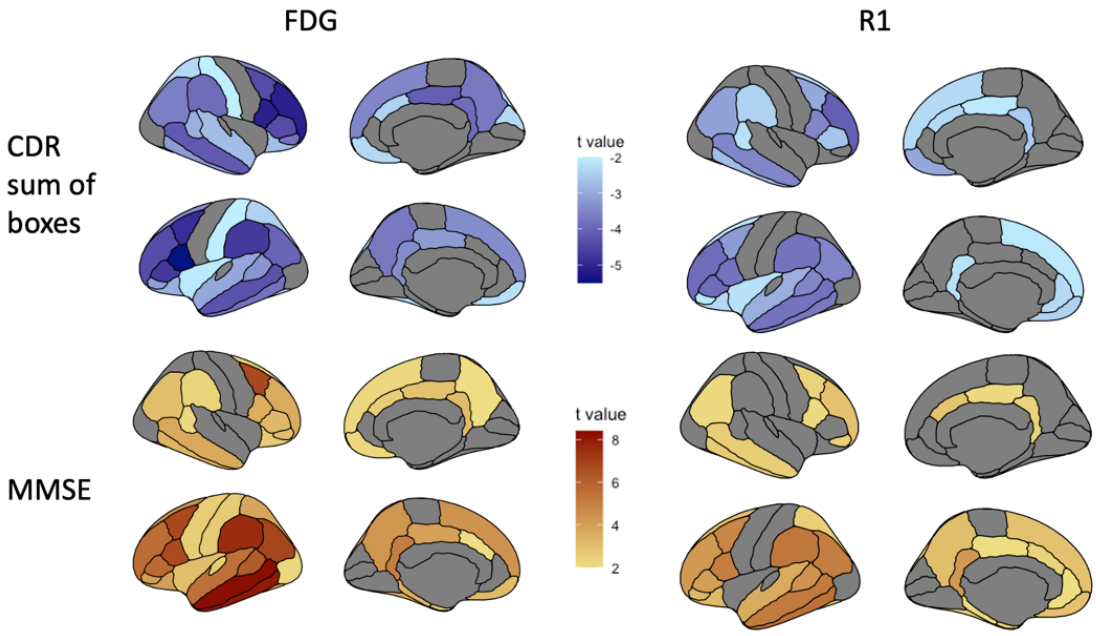

Figure 4: Associations between FDG and R1 and cognition in the patient subsample. FDG and R1 both showed significant association with CDR sum of boxes (top) and MMSE (bottom), controlling for age and sex, such that worse cognition (higher CDR-SB and lower MMSE) was associated with lower signal in temporal, parietal, and frontal regions. Associations between FDG and these cognitive measures (left) were more robust. This figure shows all regions that reached a threshold of $p < 0.05$, uncorrected, to allow us to understand the patterns of regions.

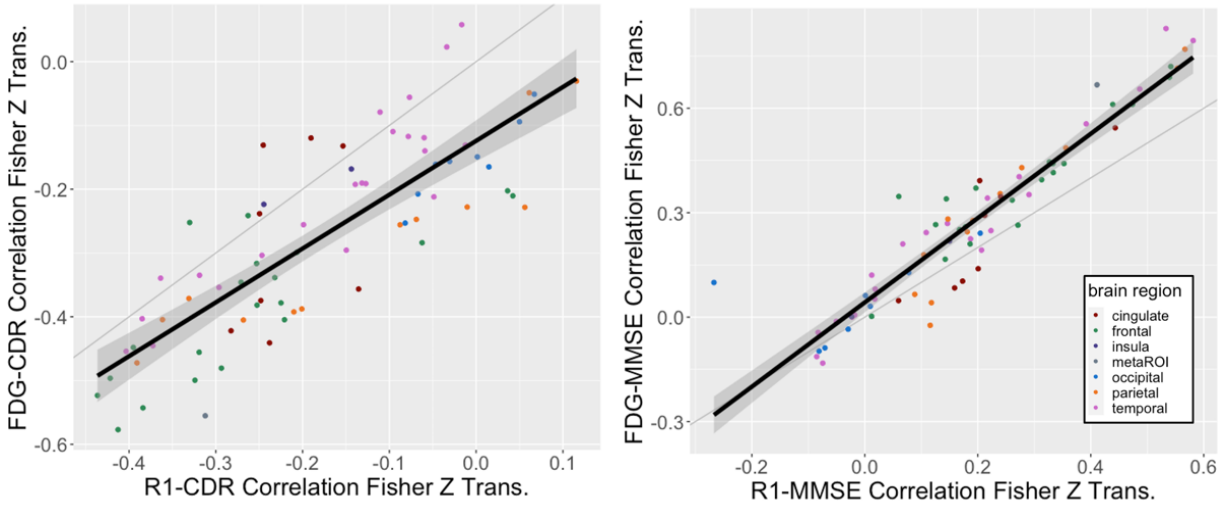

Figure 5: Correlations between Z-transformed FDG-cognition and R1-cognition relationships. Correlations were calculated for FDG/R1 in each region and CDR sum of boxes (left) and MMSE (right). Each of these correlations were Fisher *z*-transformed so the correlations across regions with both R1 and FDG could be directly compared. These measures were significantly correlated. Each dot represents the correlations in one ROI, and the ROIs are color coded by brain region.

Discussion

This study furthers our understanding of the relationship between R1 and FDG, confirming that the measures are similar and that R1 can serve as a substitute for FDG where the latter is unavailable. R1 and FDG were both lower in patients than in CNs and have a

comparable ability to discriminate between patients and Aβ- CNs. The measures show a similar relationship to MR measures of neurodegeneration and are similarly associated with cognition in patients.

Previous studies have shown high correlations between R1 and FDG (Joseph-Mathurin et al., 2018; Oliveira et al., 2018; Peretti et al., 2019) that the present study has expanded upon. To our knowledge, no paper has investigated the relationship between R1 and MRI measures of neurodegeneration. R1 and FDG had similar relationships with hippocampal volume and AD signature thickness. For hippocampal volume, the significant association in the whole sample was driven by CNs; for AD signature thickness, it was driven by patients. This may be due to a patient population which includes many individuals with earlier onset of cognitive impairments and atypical AD phenotypes more likely to affect neocortex (Ossenkoppele et al., 2016),

Both R1 and FDG were similarly associated with cognition in patients, with significant associations in temporal, frontal, and parietal regions. FDG has a more robust association with cognitive measures in this sample, although the pattern of associations is similar. There were no associations between cognitive measures and R1 and FDG in CNs, which is not unexpected given that these individuals do not experience significant neurodegeneration related to AD pathology (Jack et al., 2013a).

Many studies have previously investigated FDG as a classification tool for dementia patients (Bohnen et al., 2012; Lesman-Segev et al., 2021; Rabinovici et al., 2011). Including FDG in addition to clinical evaluation increased correct classification of pathologically confirmed AD cases versus nondemented/non-AD dementia cases (Jagust et al., 2007; Silverman et al., 2001). These studies had sensitivities over 80%, and specificities over 70%, comparable to R1 and FDG in the present study. These studies predate wide availability of Aβ-PET, which might have improved the sensitivity of these studies by confirming the presence of Aβ before autopsy in some patients who presented with no cognitive impairments, or with atypical AD symptoms. R1 in the present study was able to discriminate between patients and Aβ-negative, CN older adults slightly better than FDG and comparable to prior FDG studies. Our results reflect the performance of R1 in another, smaller study (Peretti et al., 2019).

This study has limitations. The patient sample includes many participants with atypical clinical presentations, which may have contributed to unexpected associations with cognition. In addition, the sample size for CNs with 3T MRIs was relatively small. Future studies in larger samples with more typical sporadic AD presentation would be useful to confirm the present results. Future studies comparing longitudinal trajectories of R1 and FDG would also add to our knowledge of how well R1 performs as a substitute to FDG in studies. Finally, while the R1 measures are comparable to FDG, R1 calculation requires a lengthy dynamic data acquisition which may impose difficulties in clinical situations. However, collection of more limited data may also be sufficient for estimating tracer delivery and perfusion in a dual phase protocol (Rostomian et al., 2011).

Conclusion

R1 and FDG are both lower in patients than in CN older adults and can discriminate between these groups with high accuracy. The two are also similarly associated with global measures of cognition in patients. R1 captures much of the same information as FDG, and is an appropriate measure of neurodegeneration when FDG scans are not available.

Chapter 4: Longitudinal cerebral blood flow is associated with baseline amyloid burden and tau pathology in cognitively normal older adults

Abstract

Background

Alzheimer's disease is associated with the accumulation of amyloid plaques, tau neurofibrillary tangles, and changes in cerebral blood flow (CBF), but there is debate about the temporal ordering of these changes.

Methods

Cognitively normal older adults from the Berkeley Aging Cohort Study (N=106) received two or more PIB-PET scans, from which PIB DVR, a measure of amyloid pathology, and relative delivery (R1), a measure of relative CBF to a region of interest versus a reference region, were derived. A subset of these participants (N=65) had two or more flortaucipir PET scans to measure tau pathology. Correlations between R1 and PIB DVR, and R1 and FTP, were calculated at baseline. In addition, linear mixed effects models were used to assess whether baseline FTP and PIB DVR predicted change in R1, and whether baseline R1 predicted change in FTP and PIB DVR. Finally, the association between baseline FTP, PIB DVR, and R1 with change in cognition were assessed.

Results

At baseline, PIB DVR and R1 were not correlated but higher FTP was significantly associated with lower R1. Longitudinally, higher baseline PIB DVR predicted faster decline in R1, but not vice versa. There was a trend-level association of higher baseline FTP predicting faster decreases in R1, and higher BL R1 weakly predicted faster reductions in R1. Lastly, higher FTP and PIB DVR were significantly associated with faster declines in cognition, but R1 was not related to cognitive decline.

Conclusion

Baseline amyloid pathology, measured with PIB DVR, is associated with CBF reductions, measured with R1, indicating that amyloid accumulation may precede CBF changes. The ordering of tau accumulation and CBF decline is less clear, but there is a significant association between the markers at baseline weak longitudinal associations between the variables. In terms of cognition, both amyloid pathology and tau pathology are more sensitive predictors of decline than is R1.

Introduction

Alzheimer's disease (AD) is a progressive dementia characterized by β-amyloid (Aβ) plaques, tau neurofibrillary tangles, and temporoparietal neurodegeneration. The formation of Aβ plaques is thought to be an early, if not inciting, event of AD pathogenesis, with tau accumulation and neurodegeneration occurring later in the disease (Jack et al., 2018, 2013a). An alternate theory, however, posits that vascular changes, including blood-brain barrier breakdown and ischemic events, lead to neuroinflammation, oxidative stress, impaired clearance of Aβ, and ultimately aggregation of Aβ and hyperphosphorylated tau (de la Torre and Mussivan, 1993; Scheffer et al., 2021) While many of these variables are difficult to measure during life, changes in regional cerebral blood flow (rCBF) are amenable to non-invasive measurement and can shed light on when in the pathological cascade altered cerebrovascular function may occur.

There is debate regarding whether rCBF changes in aging and dementia reflect altered vascular physiology that drives neurodegeneration, or if rCBF changes reflect reduced perfusion due to neurodegeneration reducing demand for resources (e.g., oxygen and glucose). Multiple studies have shown a tight coupling between blood flow and glucose metabolism in both humans and non-human primates (Bentourkia et al., 2000; Kuschinsky, 1991; Nihashi et al., 2007; Noda et al., 2002; Paulson et al., 2010). Furthermore, studies have shown a high correlation between [^{18}F] fluorodeoxyglucose (FDG) PET, which measures glucose metabolism, and relative delivery (R1), a measure of relative perfusion in a region of interest (ROI) versus a reference region derived from dynamic PET scans (Meyer et al., 2011; Oliveira et al., 2018; Peretti et al., 2019). Thus, it seems likely that rCBF changes, especially those measured with R1, reflect neurodegeneration that has already occurred rather than driving it.

Cross-sectional studies using various rCBF measures in humans, including arterial spin labeling (ASL) MRI and [^{15}O] H_2O Positron Emission Tomography (PET), have shown decreased CBF with worse cognition, higher amyloid load, and more impaired disease stages (Gietl et al., 2015; Leijenaar et al., 2017; Mattsson et al., 2014; Michels et al., 2016; Ottoy et al., 2019). Longitudinal studies in humans investigating whether perfusion drives amyloid accumulation, or vice versa, could help solidify which of these changes occurs first.

Further, the relationship between rCBF and tau pathology is unclear. Tau-PET and rCBF have been shown to be associated cross-sectionally with both ASL-MRI (Albrecht et al., 2020) and R1 (Visser et al., 2020). Increased tau-PET signal has also been shown to correlate with glucose hypometabolism, measured with [^{18}F] fluorodeoxyglucose (FDG) PET (Adams et al., 2019; Ossenkoppele et al., 2016; Strom et al., 2022). If rCBF changes reflect neurodegeneration, we would expect longitudinal associations between tau pathology and rCBF, which would solidify this association.

Investigating rCBF over time could help us understand when perfusion changes occur in AD. Studies of rCBF measures longitudinally are scarce, but one such study suggests R1 correlates strongly with and has higher test-retest reliability than early-frame PET data or [^{15}O] H_2O-PET (Bilgel et al., 2020). This suggests that measures of R1 could be used to examine longitudinal perfusion changes in aging and dementia.

From these studies, the question remains whether rCBF is associated cross-sectionally and longitudinally with AD biomarkers, such as Aβ and tau-PET, as well as cognitive performance. Given the conflicting hypotheses of AD pathogenesis, it is of special interest how these markers are associated early in the disease, before cognitive impairment occurs. To our knowledge, one study has investigated cross-sectional and longitudinal correlations between Aβ-PET binding potential (BP; i.e., plaque accumulation) and R1 in participants with subjective

cognitive decline. They found no cross-sectional relationship between BP and R1, but found that both baseline BP predicted longitudinal R1 and baseline R1 predicted longitudinal BP, making the inference of causality difficult (Ebenau et al., 2023). In addition, they found that low baseline R1 predicted steeper decline in cognitive performance. Another study found negative cross-sectional associations between rCBF measured with ASL-MRI and tau-PET (Albrecht et al., 2020). To our knowledge no longitudinal investigation of the relationship between these measures exists.

This study aims to investigate the relationship between relative CBF measured with R1 and other AD-PET biomarkers, as well as cognition, in cognitively normal older adults (CNs). A particular benefit of R1, in addition to its aforementioned high test-retest reliability, is that it is derived from dynamic PET scans which are often collected in research studies to measure other biomarkers (e.g. [^{11}C] Pittsburgh Compound B (PIB)-PET, which measures Aβ pathology). Thus, its use can limit study cost, as well as participant burden and radiation exposure, in studies that already collect dynamic scans.

First, we evaluated cross-sectional associations between R1 derived from PIB-PET and Aβ and tau measured by PIB distribution volume ratio (DVR) and [^{18}F] Flortaucipir (FTP)-PET measured with standard uptake value ratios (SUVRs), respectively. We predicted that R1 and PIB DVR would not be associated, but that R1 and FTP would be negatively associated, such that higher R1 would be associated with lower FTP. Next, we investigated longitudinal associations between R1 and PIB DVR/FTP. We hypothesized that higher baseline PIB DVR values would predict faster decline in R1, but that baseline R1 would not be associated with change in PIB DVR, indicating that rCBF change is downstream of amyloid accumulation, reflecting neurodegeneration and thus reduced perfusion demand. We also hypothesized that baseline FTP would be associated with change in R1, but that BL R1 would not be associated with change in FTP, indicating that aggregation of tau precedes neurodegeneration as measured through rCBF changes. Finally, we compared associations between baseline R1, FTP, and PIB DVR and cognitive performance. We predicted that higher PIB DVR and FTP would be associated with steeper decline in cognitive performance, while lower R1 would be associated with steeper decline. These results would indicate that rCBF changes are downstream of Aβ and tau accumulation, lending support to the Aβ hypothesis.

Materials and Methods

Study Participants

We recruited 106 CNs from the Berkeley Aging Cohort Study, a longitudinal study of cognitive aging (Mormino et al., 2009). All participants had longitudinal PIB scans, and a subset (N=65) had two or more FTP scans. Studies were approved by the University of California Berkeley and Lawrence Berkeley National Laboratory institutional review boards for human research.

PET Acquisition

[^{11}C] PIB was synthesized at Lawrence Berkeley National Lab (LBNL) Biomedical Isotope Facility. Study participants were injected intravenously with PIB (~15 mCi) at the beginning of a dynamic frame acquisition. Data were binned into 35 frames (4x15 seconds, 8x30 seconds, 9x60 seconds, 2x180 seconds, 10x300 seconds, and 2x600 seconds). These methods have been described previously (Lockhart et al., 2017; Mathis et al., 2003). PET data were collected on two scanners, the ECAT EXACT HR or the BIOGRAPH PET/CT Truepoint 6, and

previous analyses showed no significant difference in PIB DVRs between the scanners (Elman et al., 2014b).

[^{18}F]FTP was synthesized at LBNL based on a protocol provided by Avid Radiopharmaceuticals as previously described (Schöll et al., 2016). Data were collected 80-100 minutes after injection and were binned into 4x5 minute frames during reconstruction. All FTP scans were collected on the BIOGRAPH.

All PET images were reconstructed using an ordered subset expectation maximization algorithm with weighted attenuation, scatter correction, and smoothed with a 4mm Gaussian kernel. Patients underwent a 1.5T MRI on a Siemens Magnetom Avanto system at LBNL within a year of each PET scan. A T1-weighted magnetization prepared rapid gradient echo scan (TR/TE=2110/3.58 ms, FA=15°, 1x1×1 mm resolution) was collected during the scan that was used for coregistration. FreeSurfer (FS, https://surfer.nmr.mgh.harvard.edu/) version 5.3 was used to derive Desikan-Killiany regions of interest (ROI) from the MPRAGE, along with FS version 7.0 brainstem segmentation to define the pons as a reference region.

PET Processing

Resliced and MRI-coregistered PIB-PET images were also used for R1 calculation. R1 values were derived using SRTM2 from full-scan time activity curves in each region, with a pons reference region. In SRMT2, a global reference region clearance constant is calculated for the reference region (k'_2) within each subject to reduce noise. Three FS-derived ROIs were used: the left and right precuneus, and a metabolic metaROI (MMR) that has previously been used to capture regions of hypometabolism consisting of bilateral isthmus cingulate, middle temporal, and inferior parietal ROIs (Landau et al., 2011).

FTP SUVR ROIs were generated via mean tracer uptake 80-100 minutes after injection using an eroded white matter reference region that had been previously described (Harrison et al., 2019). SUVR images were partial volume corrected using the Geometric Transfer Matrix approach with FreeSurfer-derived values (Baker et al., 2017; Rousset et al., 1998). The primary ROI for analysis was a temporal tau metaROI (TMR) consisting of a weighted average of entorhinal, amygdala, parahippocampal gyrus, fusiform, inferior temporal, and medial temporal FreeSurfer regions (Jack et al., 2017).

Cognitive Variables

All participants receive an extensive battery of cognitive tests, from which episodic memory (EM) and executive function (EF) composites were created via confirmatory factor analysis as previously described (Dobyns et al., 2021). Data from visits concurrent with and following imaging visits were used. As such, a different cognitive visit was used as baseline for PIB and FTP analyses.

Statistical Analyses

Statistical analyses were conducted using MATLAB version 9.7 (R2019b; MathWorks, Inc., Natick, Massachusetts) and R version 4.2.0 (https://www.R-project.org/), including the packages *nlme* for linear mixed-effects models and *sjPlot* and *ggplot2* for data visualization.

For cross-sectional analyses, linear models controlling for age and sex were used to investigate associations between the variables at baseline. For longitudinal imaging marker analyses, four longitudinal mixed effects models (LMEMs) were set up: baseline PIB DVR predicting longitudinal R1, baseline R1 predicting longitudinal PIB DVR, baseline FTP predicting longitudinal R1, and baseline R1 predicting longitudinal FTP. In these models, the

longitudinal variable was the dependent variable, with fixed effects of the baseline variable, baseline age, and sex, all interacting with time. The random effects were (1+time|subject), which modeled subject-specific intercepts.

For cognition analyses, LMEMs were set up with the cognitive variable as the dependent variable, and fixed effects of the baseline imaging marker (PIB DVR, R1, and FTP), baseline age, and sex, all interacting with time. As with the imaging-only analyses, the random effects were (1+time|subject). All statistics are reported at a liberal threshold of $p<0.05$, uncorrected.

Results

Participant Characteristics and Descriptive Statistics

Participants had a mean age of approximately 75 years in the total sample (N = 106), and FTP subset (N = 65). Half of the participants in the sample (53/106) had two PIB scans, while the rest had three or more, with a mean follow-up time of 4.69 years. The FTP sample had a mean follow-up time of 2.62 years, with approximately two-thirds (42/65) of participants having two scan time points with matched PIB and FTP scans, while the remaining participants had three or four scans. Number of cognitive visits ranged from 2 to 13 for the entire sample, and 2 to 7 in the FTP subset. The mean follow-up time was 7.26 years for the whole sample, and 4.64 years in the FTP subset. Additional participant characteristics can be seen in **Table 1.**

	All	**FTP subset**
Subjects	N = 106	N = 65
BL age	75.00 ± 5.13	74.73 ± 4.97
Years of followup	4.69 ± 3.07	2.62 ± 1.27
Sex (F/M)	66/40	39/26
BL PIB status (-/+)	66/40	40/25
Average BL PIB DVR	1.12 ± 0.19	1.12 ± 0.19
Number of PIB scans:	2 scans: 53 3 scans: 36 4 scans: 13 5 scans: 4	2 scans: 42 3 scans: 21 4 scans: 2
Years of NP followup	7.26 ± 3.39	4.64 ± 2.07
Number of NP visits	2 visits: 8 3 visits: 13 4 vis: 18 5 visits: 13 6 visits:11 7 visits:10 8 visits: 8 9 visits: 9 10 visits: 6 11 visits: 8 12 visits: 2 13 visits: 1	2visits: 5 3 visits: 16 4 visits: 16 5 visits: 12 6 visits: 8 7 visits: 8

Table 1: Subject Demographics and descriptive statistics
A summary of all study participants. Participants in the FTP-PET subset are all included in the main sample. Continuous variables are reported as mean ± standard deviation.

Imaging Analyses

At baseline, PIB DVR and MMR R1 were not significantly associated (t(102) = -0.70, p = 0.5), controlling for age and sex. There was also no significant difference in R1 MMR between PIB+ and PIB- participants in a two-sample t-test with a cutoff DVR of 1.065 (t(87) = -0.29, p = 0.7). However, tau in the TMR and R1 in the MMR were significantly associated (t(60) = -2.08, p = 0.04) such that higher FTP SUVR was associated with lower R1. These data are shown in **Figure 1.**

Longitudinally, PIB DVR and R1 were associated. Trajectories of PIB DVR and R1 for each subject are shown as spaghetti plots in **Figures 2a** and **2b**, respectively. Controlling for age and sex, baseline MMR R1 did not predict change in PIB (BL R1 * time term: t(176) = -1.23, p = 0.22; **Figure 2c**). Baseline PIB DVR, however, weakly predicted change in R1 in the MMR (BL PIB DVR * time term: t(176) = -1.91, p = 0.058; **Figure 2d**) and significantly predicted change in the precuneus, both in the left (BL PIB DVR * time term: t(176) = -2.22, p = 0.028; **Figure 2e**) and right (BL PIB DVR * time term: t(176) = -2,37, p = 0.019) hemispheres.

The relationship between longitudinal FTP and R1 is less clear. Trajectories of FTP SUVR and R1 are shown in **Figures 3a** and **3b.** As visualized in **Figure 3c** and **3d**, baseline MMR R1 is not related to change in TMR FTP SUVR (BL R1 * time term: t(84) = -1.27, p = 0.21) but lower baseline left precuneus R1 is associated with faster increases in TMR FTP SUVR (BL R1 * time term: t(84) = -1.99, p = 0.050). Baseline temporal FTP in TMR does not predict change in R1 in MMR, although the relationship does show a trend toward significance (BL FTP * time term: t(84) = -1.62, p = 0.11; **Figure 3e**).

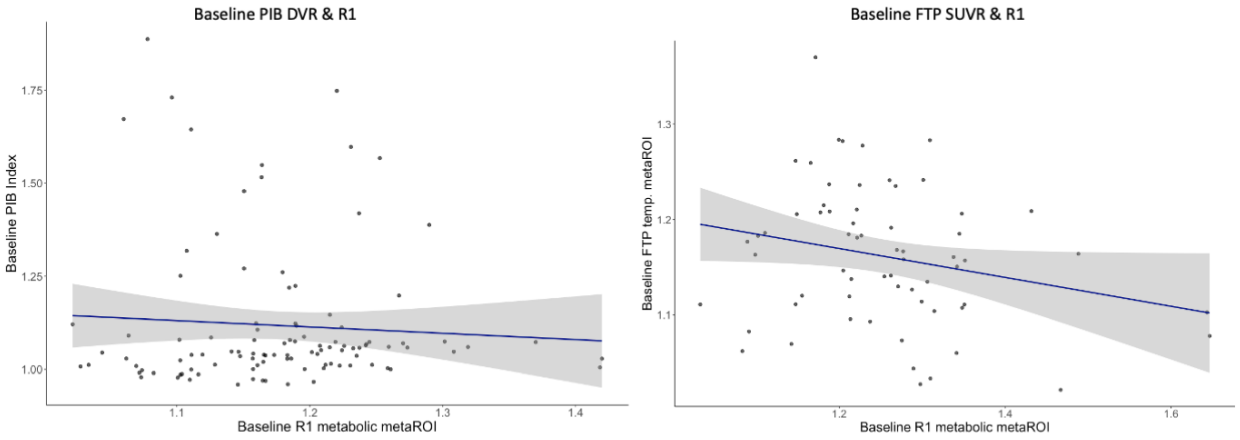

Figure 1: Cross-sectional R1-PIB DVR/FTP relationships
Cross-sectional associations between R1 and PIB DVR (left) and FTP (left). Controlling for age and sex, R1 and PIB DVR were not significantly associated (t(102) = -0.70, p = 0.5); R1 and FTP did have a significant relationship t(60) = -2.08, p =

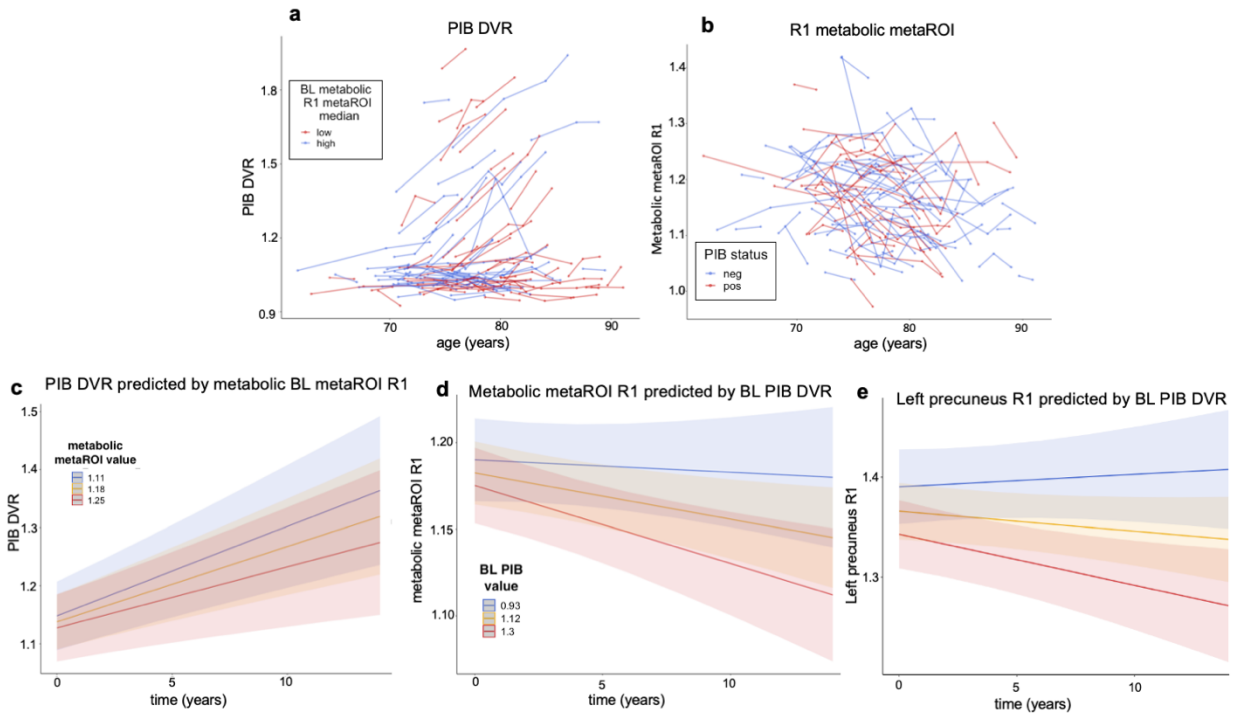

Figure 2: Longitudinal R1-PIB DVR relationships
Spaghetti plots of each subjects' trajectory on each variable are shown in **2a** and **2b**. Baseline MMR R1 did not significantly predict change in PIB DVR (**2c**; t(176) = -1.23, p = 0.22). Baseline PIB DVR weakly predicted change3 in MMR R1 (**2d**; t(176) = -1.91, p = 0.058) and significantly predicted change in the left and right precuneus (left precuneus shown; **2e**; t(176) = -2.22, p = 0.028).

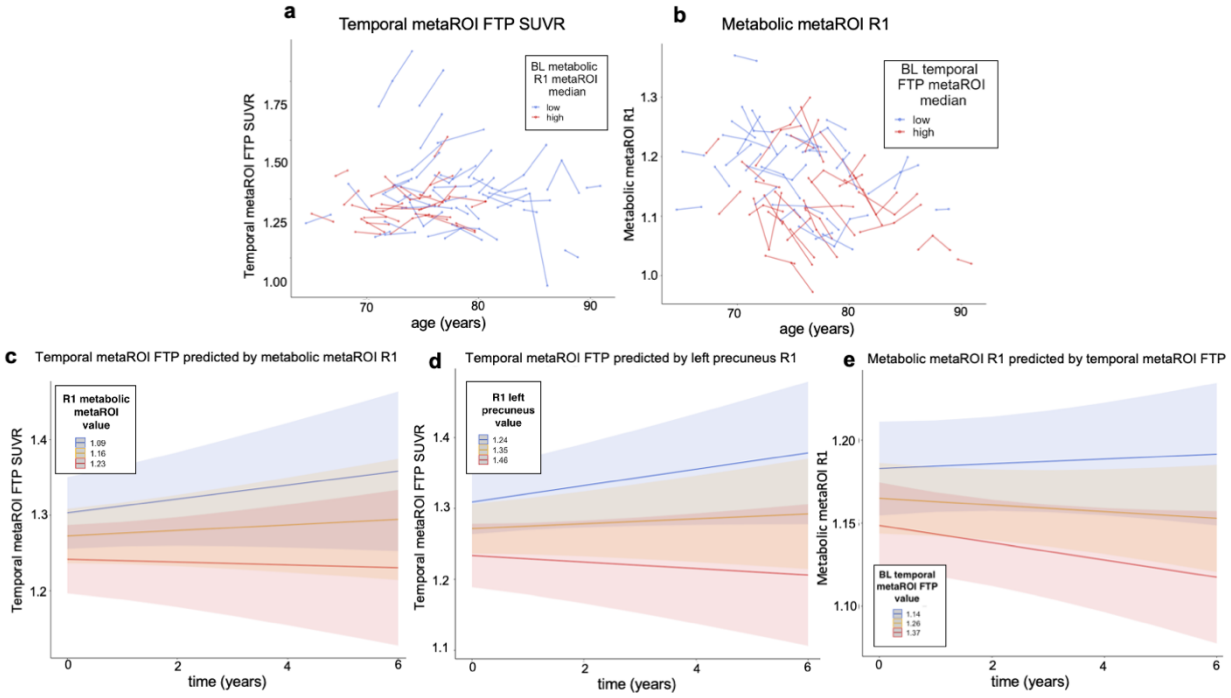

Figure 3: Longitudinal R1-FTP relationships
Spaghetti plots of each subjects' trajectory on each variable are shown in **3a** and **3b**. Baseline MMR R1 is not related to change in MMR FTP (**3c**; t(84) = -1.27, p = 0.21), but baseline left precuneus R1 weakly predicts change in TMR FTP (**3d**; t(84) = -1.99, p = 0.050). Baseline TMR FTP does not significantly predict MMR R1, although there is a weak trend-level association (**3e**; t(84) = -1.62, p = 0.11)

Cognition Analyses

Baseline PIB DVR and temporal metaROI FTP are associated with change in composite scores in both EM (PIB DVR * time term: t(540) = -3.44, p = 0.006); FTP * time term: t(216) = -3.01, p = 0.003) and EF (PIB DVR * time term: t(540) = -3.89, p = 0.0001); FTP * time term: t(216) = -2.59, p = 0.001). PIB DVR remained significantly associated with cognition in the FTP subsample (EM: t(216) = -2.69, p = 0.008); EF: t(216) = -2.50, p = 0.013). For both variables, higher baseline values are related to faster decline in cognitive score.

Baseline R1, however, is not associated with decline in either cognitive composite variable in either the metabolic metaROI or precuneus (metabolic metaROI R1* time term predicting EM: t(540) = 0.54, p = 0.54; EF: t(540) = 0.37; p = 0.71). The associations are the same in the FTP subset. These results can be seen in **Figure 4.**

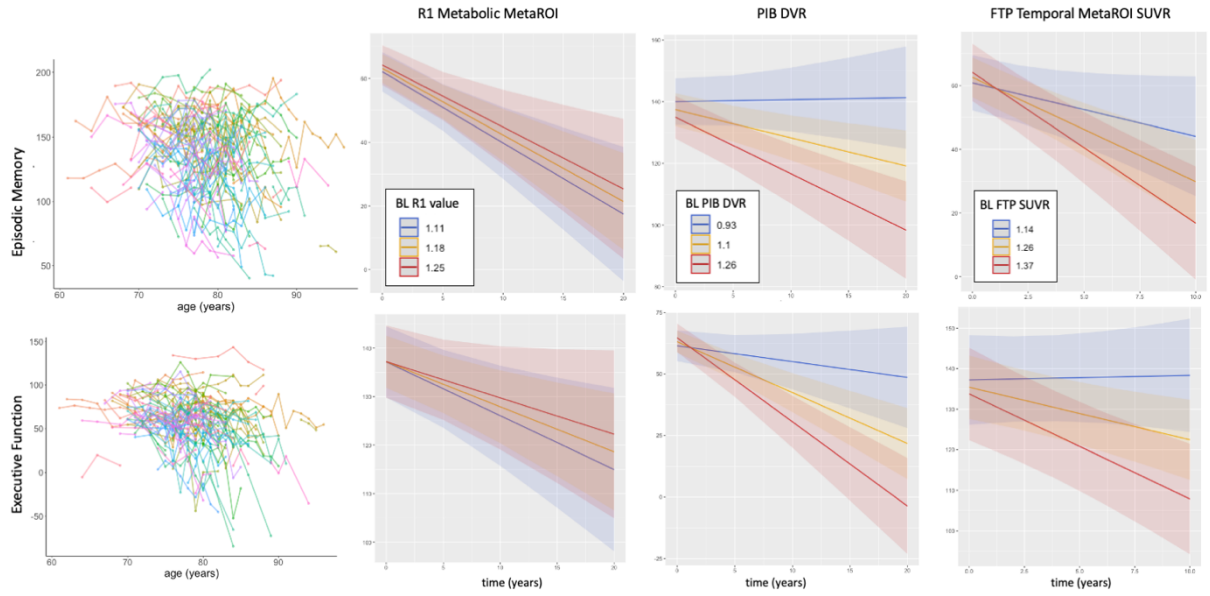

Figure 4: Baseline PET-longitudinal cognition analyses
Spaghetti plots of each subjects' trajectory for each cognitive variable are shown in the far left column, with EM on top and EF on the bottom. MMR R1 was not significantly associated with cognitive decline in either variable (middle left; EM: t(540) = 0.54, p = 0.54; EF: t(540) = 0.37; p = 0.71). Both PIB DVR (middle right; EM: t(540) = -3.44, p = 0.006; EF: t(540) = -3.89, p = 0.0001) and TMR FTP (far right; EM: t(216) = -3.01, p = 0.003; EF: t(216) = -3.01, p = 0.003).

Discussion

In this study, we investigated the associations between PIB R1, a proxy of cerebral blood flow, and both PIB DVR and FTP, measures of amyloid and tau pathology, respectively. We examined the cross-sectional associations between R1 and PIB DVR/FTP and found that baseline R1 was associated with baseline FTP, but not with baseline PIB DVR. Next, we studied longitudinal associations with an interest in understanding if we could make inferences about directionality from these analyses. We found that baseline PIB DVR predicted change in R1 such that higher baseline PIB was associated with faster decline in R1, but not vice versa, indicating that amyloid deposition precedes changes in cerebral blood flow.

Longitudinal relationships between R1 and tau are more unclear. Low baseline R1 has a weak association with steeper increases in FTP, and there seems to be a slight trend-level

association between higher baseline FTP and steeper decreases in R1. One possibility is that the two processes are related enough that it is difficult to detect a direction of the association in data with relatively short periods of follow up. It is also possible that perfusion drives tau deposition, or that there is a bi-directional relationship.

Unlike FTP and PIB DVR, R1 was, rather surprisingly, not associated with change in cognitive performance, indicating that these two measures are more sensitive to cognitive decline. Taken together, these results further our understanding of how cerebral blood flow is associated with AD biomarkers and cognition in cognitively normal older adults.

Cerebral Blood Flow and Aβ Pathology

At baseline, PIB DVR and R1 were not correlated, nor did PIB+ and PIB- participants have different R1 levels at baseline. This indicates no cross-sectional relationship between Aβ and cerebral blood flow in cognitively normal older adults. This stands in contrast to some studies, which have found that higher Aβ is associated with lower rCBF, sometimes independent of diagnostic group (Mattsson et al., 2014) and sometimes in only the Aβ+ participants (Bangen et al., 2017; Bilgel et al., 2020; Michels et al., 2016; Sojkova et al., 2008). Other studies have found the opposite effect, that, in Aβ+ participants in particular, higher Aβ burden was correlated with higher rCBF (Bangen et al., 2017; Fazlollahi et al., 2020), which we also found no evidence for. However, other studies found no association between Aβ and rCBF at baseline (Gietl et al., 2015), two of which notably feature only unimpaired participants as in this study (Bangen et al., 2017; Ebenau et al., 2023). Studies with differing findings mostly include participants with cognitive impairment, and thus have a wider range of Aβ pathology and rCBF values that may lead to more sensitivity in detecting differences. Cross-sectional results alone, however, do not provide sufficient evidence to conclude that perfusion doesn't drive amyloid; it may instead be the case that CN participants lack sufficient pathology to detect an effect. Thus, we look to our longitudinal analyses.

Longitudinally, we found that baseline PIB DVR predicted change in R1, but not vice versa. Individuals who had higher Aβ at baseline had faster declines in rCBF, but baseline rCBF did not predict change in Aβ. These findings conflict with another study which used Aβ-PET and R1, which found a bidirectional relationship (Ebenau et al., 2023). Ebenau and colleagues theorized, based on this result, that there may be early vascular effects exerted on Aβ accumulation in addition to Aβ pathology driving faster reductions in rCBF. We only found evidence for the latter conclusion. In addition, we did not find any evidence for compensatory mechanisms, such as increasing rCBF being associated with higher Aβ. Our results indicate that Aβ accumulation likely precedes deficits in rCBF and thus lends credence to the amyloid hypothesis, and the notion that rCBF measures in aging and dementia more likely reflect neurodegeneration, rather than vascular changes which are an inciting factor in AD.

Cerebral Blood Flow and Tau Pathology

Cross-sectionally, baseline FTP and R1 were correlated, which is in line with previous findings (Albrecht et al., 2020; Visser et al., 2020), but our longitudinal results were less straightforward. We found that baseline FTP had a trend-level association in predicting faster decline in R1, and that lower baseline left precuneus R1 weakly predicted faster increases in FTP. Our findings indicate that there is an association between rCBF and tau pathology, but it is not completely clear in this sample if rCBF or tau occurs earlier, or if they occur at roughly the same time. Studies with larger sample sizes and individuals with cognitive impairment may be able to further elucidate this relationship.

Change in Cognition Associated with Aβ, tau and CBF

In this sample, higher baseline PIB DVR and higher baseline FTP both predicted faster rates of cognitive decline in an episodic memory and executive function composite. These findings are in line with previous studies investigating cognitive decline in association with amyloid pathology (Doraiswamy et al., 2012; Farrell et al., 2017) and tau pathology (Biel et al., 2021; Lagarde et al., 2022; Teng et al., 2021). R1, however, showed no significant associations with decline in cognition. Thus, at least in the current sample, both Aβ and tau pathology are more sensitive predictors of cognitive performance than rCBF measured with R1. This stands in contrast with a recent study, which found that R1 predicted cognitive decline (Ebenau et al., 2023). It is unclear why our results contradict these previous findings, but it is possible that a wider range of cognitive function, through the inclusion of participants with subjective cognitive decline, might explain the discrepancy.

Limitations and Future Directions

As previously mentioned, this study included only cognitively normal individuals, and included a somewhat limited sample size. Though it is notable that we found Aβ- and tau-rCBF relationships given this, some of our associations may be more robust in a larger sample with longer follow-up time and individuals exhibiting cognitive impairment. Having a larger sample would also supply additional power to see if relationships differ by Aβ status.

Conclusion

In this study, we found evidence that Aβ pathology precedes CBF changes, and that tau pathology and CBF are related, in cognitively normal older adults. We also found that Aβ and tau pathology at baseline predict cognitive decline, but that R1-measured CBF does not.

Chapter 5: Discussion

This dissertation utilizes multimodal neuroimaging data and cognitive assessments to further our understanding of AD PET biomarkers and the temporal dynamics of AD-related pathological changes, with a particular focus on Aβ and neurodegeneration measures. **Chapter 2** demonstrates that Aβ pathology accumulation rates across brain regions peak during an 8-year period. **Chapter 3** confirms the utility of R1 as a biomarker of neurodegeneration that is highly correlated with FDG cross-sectionally, and **Chapter 4** demonstrates that changes in R1-measured CBF are downstream of Aβ aggregation. These results indicate that widespread Aβ accumulation is an early event in the AD pathological cascade, with followed by neurodegeneration measures, including CBF and FDG.

Aβ pathology is widespread even in preclinical AD

Previous studies attempting to identify early loci of Aβ pathology have shown a variety of regions, mostly in frontal, parietal, and lateral temporal regions (Cho et al., 2016; Grothe et al., 2017; Guo et al., 2017; Mattsson et al., 2019; Palmqvist et al., 2017; Yotter et al., 2013). Our results from **Chapter 2** found that parietal and frontal regions were among the first to reach their peak accumulation rates, but that all regions reached peak accumulation rates in under decade. Notably, we were able to find these results using a cognitively normal cohort, which may be why our time to peak accumulation may be prolonged compared to other studies (Jagust and Landau, 2021). In general, it seems likely that all regions begin to harbor Aβ pathology at approximately the same time, but that rates of accumulation may be the result of different carrying capacities and local tissue properties, as posited by Whittington et al. (2018). In general, medial temporal and sensorimotor regions seem to have lower susceptibility, but other cortical regions may ultimately have similar levels of Aβ, and PET studies staging Aβ pathology may find a different subset of these regions show accumulation earliest based on factors such as subject demographics, clinical status, and PET tracer. The underlying factors driving regional susceptibility to Aβ may be related to widely-shared tissue characteristics such as mitochondrial respiration or aerobic glycolysis (Grothe et al., 2018; Vlassenko et al., 2010).

Our results comparing regional Aβ inAPOE ε4 allele carriers versus noncarriers and investigating the effect of rates of Aβ accumulation on tau pathology provided further evidence that Aβ pathology in all brain regions is associated similarly with AD risk and pathology. Across all regions, APOE ε4 carriers had higher rates of change in Aβ. Furthermore, faster rates of regional Aβ accumulation were associated with tau pathology in the same subset of primarily temporal and parietal regions. This builds upon previous cross-sectional results from the lab, showing that higher Aβ in a broad range of regions was associated with increased temporoparietal tau (Lockhart et al., 2017).

These results point to the potential need for different methods to identify early Aβ accumulation. Until there is a reliable way to measure oligomeric Aβ *in vivo*, perhaps utilizing CSF measures of Aβ, which precede Aβ-PET measures in becoming abnormal, in concert with some measure of Aβ-PET, or utilizing spatial extent to account for potential individual differences in early loci Aβ deposition (Farrell et al., 2022) may show greater promise as a marker of earlier Aβ.

Cros-sectionally, R1-measured CBF is highly correlated with hypometabolism

Temporoparietal hypometabolism is a well-known phenomenon of AD observed via FDG scans (Nordberg et al., 2010), but many research studies do not currently collect FDG scans in CN older adult cohorts. Previous studies have established that R1, a CBF proxy which can be derived from dynamic PET scans which are readily available in many research studies, including BACS, are highly correlated with FDG (Meyer et al., 2011; Oliveira et al., 2018; Peretti et al., 2019; Rodriguez-Vieitez et al., 2017). These studies, however, have not demonstrated a relationship between R1 and MRI measures of neurodegeneration, which often show relatively weak agreement with FDG when dichotomizing subjects into groups (Jack et al., 2015). **Chapter 3** not only confirms that R1 is highly correlated with FDG, but also that it is highly correlated with cortical thickness in AD-vulnerable regions. Its association with hippocampal volume was weaker, but importantly, both hippocampal volume and AD-signature thickness showed similar correlations with FDG and R1. Furthermore, regional R1 and FDG showed similar patterns of association with clinical severity in cognitively impaired participants, though R1 was a less sensitive measure of clinical performance than FDG. We did not find significant differences between Aβ+ and Aβ- CNs in FDG or R1, indicating that CBF and hypometabolism may be a later development in the AD pathological cascade, which is consistent with models of the disease (Jack et al., 2013a).

This confirmation of R1 as a useful measure of neurodegeneration could be important in research studies and, potentially, in the clinic. Calculating R1 from Aβ-PET scans, as is done here, allows for the extraction of multiple variables of interest—CBF and Aβ burden—from a single scan. In research studies that already have dynamic PET data, R1 can be calculated without any additional cost or patient burden. In clinical settings, however, the long acquisition time of dynamic PET data makes R1 a less appealing measure. Dual-phase protocols, where tracer wash-in is imaged, followed by a waiting period outside the scanner, then scanning is recommenced once a steady state has been reached to see tracer binding to the receptor of interest, has been shown to be less sensitive than R1 (Joseph-Mathurin et al., 2018; Peretti et al., 2019), but more extensive research into its correlations with cognition, PET- and fluid-based biomarkers, and MRI markers of neurodegeneration may confirm its utility as a clinical alternative to FDG.

Longitudinally, R1-measured CBF is an indicator of neurodegeneration

The vascular hypothesis of AD posits that early vascular damage causes AD (de la Torre and Mussivan, 1993; Scheffer et al., 2021). Our final project in **Chapter 4** investigated associations between cross sectional and longitudinal associations between R1 and both PIB DVR and FTP, to establish if R1-measured CBF could be staged relative to Aβ and tau pathology. We found no cross-sectional association between Aβ and R1. Baseline Aβ predicted change in CBF, but not the reverse. This stands in contrast to a recent study that found a bidirectional association between the two variables (Ebenau et al., 2023); our study includes more participants, a longer follow-up time, and more study visits, on average, which allows us to better model the longitudinal trajectories of each variable. Our results indicate that R1 changes follow changes in Aβ, placing R1-measured CBF after Aβ in the pathological cascade and supporting the Aβ cascade hypothesis over the vascular hypothesis of AD. Relationships between R1-measured CBF and tau were murkier; at baseline, the two variables were negatively correlated, and low baseline R1 was associated with steeper increases in tau. There was also a trend-level relationship between higher baseline tau and steeper increases in left precuneus R1. Finally, baseline R1 was not associated with change in cognition, while both Aβ and tau were.

These results indicate a clear relationship between Aβ and CBF, such that Aβ pathology precedes CBF, and indicates CBF, at least measured with R1, is more likely a measure of neurodegeneration than one sensitive to early vascular change that precedes Aβ accumulation. Further study of the relationships between R1-measured CBF and tau would benefit from studies with longer follow up and cohorts with more diversity in cognitive performance to tease apart the directionality of the association, if there is one.

Conclusion

This dissertation furthers our understanding of the pathological cascade in preclinical AD. **Chapter 2** provides evidence that Aβ pathology, at least at the level of fibrillar insoluble plaques, accumulates in a large suite of frontal and parietal regions on a similar time scale, lending credence to the idea that Aβ pathology is not spreading slowly from one brain region to another but rather appearing simultaneously in multiple regions. All Aβ regions were similarly related to temporoparietal tau pathology and sporadic AD genetic risk. **Chapter 4** demonstrates that CBF change is a later phenomenon in AD which follows global Aβ deposition and is associated more closely cross-sectionally with tau. **Chapter 3** provides evidence that R1-measured CBF is a proxy of neurodegeneration and is associated cross-sectionally with measures of hypometabolism and MRI measures of neurodegeneration, further establishing R1 as a marker of neurodegeneration and establishing the utility of dynamic PET scans as dual-use markers of the tracer's target receptor and CBF/neurodegeneration.

References

Adams, J.N., Lockhart, S.N., Li, L., Jagust, W.J., 2019. Relationships between tau and glucose metabolism reflect alzheimer's disease pathology in cognitively normal older adults. Cereb. Cortex 29, 1997–2009. https://doi.org/10.1093/cercor/bhy078

Albrecht, D., Isenberg, A.L., Stradford, J., Monreal, T., Sagare, A., Pachicano, M., Sweeney, M., Toga, A., Zlokovic, B., Chui, H., Joe, E., Schneider, L., Conti, P., Jann, K., Pa, J., 2020. Associations between vascular function and tau PET are associated with global cognition and amyloid. J. Neurosci. 40, JN-RM-1230-20. https://doi.org/10.1523/jneurosci.1230-20.2020

Baker, S.L., Maass, A., Jagust, W.J., 2017. Considerations and code for partial volume correcting [18F]-AV-1451 tau PET data. Data Brief 15, 648–657. https://doi.org/10.1016/j.dib.2017.10.024

Bangen, K.J., Clark, A.L., Edmonds, E.C., Evangelista, N.D., Werhane, M.L., Thomas, K.R., Locano, L.E., Tran, M., Zlatar, Z.Z., Nation, D.A., Bondi, M.W., Delano-Wood, L., 2017. Cerebral Blood Flow and Amyloid-β Interact to Affect Memory Performance in Cognitively Normal Older Adults. Front. Aging Neurosci. 9, 181. https://doi.org/10.3389/fnagi.2017.00181

Bentourkia, M., Bol, A., Ivanoiu, A., Labar, D., Sibomana, M., Coppens, A., Michel, C., Cosnard, G., De Volder, A.G., 2000. Comparison of regional cerebral blood flow and glucose metabolism in the normal brain: effect of aging. J. Neurol. Sci. 181, 19–28. https://doi.org/10.1016/S0022-510X(00)00396-8

Biel, D., Brendel, M., Rubinski, A., Buerger, K., Janowitz, D., Dichgans, M., Franzmeier, N., for the Alzheimer's Disease Neuroimaging Initiative (ADNI), 2021. Tau-PET and in vivo Braak-staging as prognostic markers of future cognitive decline in cognitively normal to demented individuals. Alzheimers Res. Ther. 13, 137. https://doi.org/10.1186/s13195-021-00880-x

Bilgel, M., Beason-Held, L., An, Y., Zhou, Y., Wong, D.F., Resnick, S.M., 2020. Longitudinal evaluation of surrogates of regional cerebral blood flow computed from dynamic amyloid PET imaging. J. Cereb. Blood Flow Metab. 40, 288–297. https://doi.org/10.1177/0271678X19830537

Blautzik, J., Brendel, M., Sauerbeck, J., Kotz, S., Scheiwein, F., Bartenstein, P., Seibyl, J., Rominger, A., 2017. Reference region selection and the association between the rate of amyloid accumulation over time and the baseline amyloid burden. Eur. J. Nucl. Med. Mol. Imaging 44, 1364–1374. https://doi.org/10.1007/s00259-017-3666-8

Bohnen, N.I., Djang, D.S.W., Herholz, K., Anzai, Y., Minoshima, S., 2012. Effectiveness and Safety of ^{18}F-FDG PET in the Evaluation of Dementia: A Review of the Recent Literature. J. Nucl. Med. 53, 59–71. https://doi.org/10.2967/jnumed.111.096578

Braak, H., Braak, E., 1991. Neuropathological stageing of Alzheimer-related changes. Acta Neuropathol. (Berl.) 82, 239–259. https://doi.org/10.1007/BF00308809

Burnham, S.C., Laws, S.M., Budgeon, C.A., Doré, V., Porter, T., Bourgeat, P., Buckley, R.F., Murray, K., Ellis, K.A., Turlach, B.A., Salvado, O., Ames, D., Martins, R.N., Rentz, D., Masters, C.L., Rowe, C.C., Villemagne, V.L., 2020. Impact of APOE-ε4 carriage on the onset and rates of neocortical Aβ-amyloid deposition. Neurobiol. Aging 95, 46–55. https://doi.org/10.1016/j.neurobiolaging.2020.06.001

Chetelat, G., Villemagne, V.L., Villain, N., Jones, G., Ellis, K.A., Ames, D., Martins, R.N., Masters, C.L., Rowe, C.C., On behalf of the AIBL Research Group, 2012. Accelerated cortical atrophy in cognitively normal elderly with high -amyloid deposition. Neurology 78, 477–484. https://doi.org/10.1212/WNL.0b013e318246d67a

Cho, H., Choi, J.Y., Hwang, M.S., Kim, Y.J., Lee, H.M., Lee, H.S., Lee, J.H., Ryu, Y.H., Lee, M.S., Lyoo, C.H., 2016. In vivo cortical spreading pattern of tau and amyloid in the Alzheimer disease spectrum. Ann. Neurol. 80, 247–258. https://doi.org/10.1002/ana.24711

de la Torre, J.C., Mussivan, T., 1993. Can disturbed brain microcirculation cause Alzheimer's disease? Neurol. Res. 15, 146–153. https://doi.org/10.1080/01616412.1993.11740127

de Leon, M.J., Convit, A., Wolf, O.T., Tarshish, C.Y., DeSanti, S., Rusinek, H., Tsui, W., Kandil, E., Scherer, A.J., Roche, A., Imossi, A., Thorn, E., Bobinski, M., Caraos, C., Lesbre, P., Schlyer, D., Poirier, J., Reisberg, B., Fowler, J., 2001. Prediction of cognitive decline in normal elderly subjects with 2-[^{18} F]fluoro-2-deoxy- D -glucose/positron-emission tomography (FDG/PET). Proc. Natl. Acad. Sci. 98, 10966–10971. https://doi.org/10.1073/pnas.191044198

Dobyns, L., Zhuang, K., Baker, S.L., Jagust, W.J., Harrison, T.M., 2021. A global resilience score captures associations with AD pathology and predicts cognitive decline in cognitively healthy older adults. Alzheimers Dement. 17. https://doi.org/10.1002/alz.052302

Doraiswamy, P.M., Sperling, R.A., Coleman, R.E., Johnson, K.A., Reiman, E.M., Davis, M.D., Grundman, M., Sabbagh, M.N., Sadowsky, C.H., Fleisher, A.S., Carpenter, A., Clark, C.M., Joshi, A.D., Mintun, M.A., Skovronsky, D.M., Pontecorvo, M.J., For the AV45-A11 Study Group, 2012. Amyloid- assessed by florbetapir F 18 PET and 18-month cognitive decline: A multicenter study. Neurology 79, 1636–1644. https://doi.org/10.1212/WNL.0b013e3182661f74

Ebenau, J.L., Visser, D., Verfaillie, S.C.J., Timmers, T., van Leeuwenstijn, M.S.S.A., Kate, M. ten, Windhorst, A.D., Barkhof, F., Scheltens, P., Prins, N.D., Boellaard, R., van der Flier, W.M., van Berckel, B.N.M., 2023. Cerebral blood flow, amyloid burden, and cognition in cognitively normal individuals. Eur. J. Nucl. Med. Mol. Imaging 50, 410–422. https://doi.org/10.1007/s00259-022-05958-8

Elman, J.A., Oh, H., Madison, C.M., Baker, S.L., Vogel, J.W., Marks, S.M., Crowley, S., O'Neil, J.P., Jagust, W.J., 2014a. Neural compensation in older people with brain amyloid-β deposition. Nat. Neurosci. 17, 1316–1318. https://doi.org/10.1038/nn.3806

Elman, J.A., Oh, H., Madison, C.M., Baker, S.L., Vogel, J.W., Marks, S.M., Crowley, S., O'Neil, J.P., Jagust, W.J., 2014b. Neural compensation in older people with brain amyloid-β deposition. Nat. Neurosci. 17, 1316–1318. https://doi.org/10.1038/nn.3806

Farrell, M.E., Kennedy, K.M., Rodrigue, K.M., Wig, G., Bischof, G.N., Rieck, J.R., Chen, X., Festini, S.B., Devous, M.D., Park, D.C., 2017. Association of Longitudinal Cognitive Decline With Amyloid Burden in Middle-aged and Older Adults: Evidence for a Dose-Response Relationship. JAMA Neurol. 74, 830. https://doi.org/10.1001/jamaneurol.2017.0892

Farrell, M.E., Thibault, E.G., Becker, A., Price, J.C., Schultz, A.P., Properzi, M.J., Buckley, R.F., Jacobs, H.I.L., Hanseeuw, B., Sperling, R.A., Johnson, K.A., 2022. Optimizing early detection of beta-amyloid accumulation with PET using spatial extent. Alzheimers Dement. 18. https://doi.org/10.1002/alz.068029

Fazlollahi, A., Calamante, F., Liang, X., Bourgeat, P., Raniga, P., Dore, V., Fripp, J., Ames, D., Masters, C.L., Rowe, C.C., Connelly, A., Villemagne, V.L., Salvado, O., for the Australian Imaging Biomarkers and Lifestyle (AIBL) Research Group, 2020. Increased cerebral blood flow with increased amyloid burden in the preclinical phase of alzheimer's disease. J. Magn. Reson. Imaging 51, 505–513. https://doi.org/10.1002/jmri.26810

Folstein, M.F., Folstein, S.E., McHugh, P.R., 1975. "Mini-mental state". A practical method for grading the cognitive state of patients for the clinician. J. Psychiatr. Res. 12, 189–198. https://doi.org/10.1016/0022-3956(75)90026-6

Fouquet, M., Besson, F.L., Gonneaud, J., Joie, R.L., Chételat, G., 2014. Imaging Brain Effects of APOE4 in Cognitively Normal Individuals Across the Lifespan. Neuropsychol. Rev. 24, 290–299. https://doi.org/10.1007/s11065-014-9263-8

Frankish, H., Horton, R., 2017. Prevention and management of dementia: a priority for public health. The Lancet 390, 2614–2615. https://doi.org/10.1016/S0140-6736(17)31756-7

Geula, C., Wu, C.-K., Saroff, D., Lorenz, A., Yuan, M., Ankner, B.A.Y., 1998. Aging renders the brain vulnerable to amyloid B-protein neurotoxicity 4, 827–831.

Gietl, A.F., Warnock, G., Riese, F., Kälin, A.M., Saake, A., Gruber, E., Leh, S.E., Unschuld, P.G., Kuhn, F.P., Burger, C., Mu, L., Seifert, B., Nitsch, R.M., Schibli, R., Ametamey, S.M., Buck, A., Hock, C., 2015. Regional cerebral blood flow estimated by early PiB uptake is reduced in mild cognitive impairment and associated with age in an amyloid-dependent manner. Neurobiol. Aging 36, 1619–1628. https://doi.org/10.1016/j.neurobiolaging.2014.12.036

Götz, J., Streffer, J.R., David, D., Schild, A., Hoerndli, F., Pennanen, L., Kurosinski, P., Chen, F., 2004. Transgenic animal models of Alzheimer's disease and related disorders: histopathology, behavior and therapy. Mol. Psychiatry 9, 664–683. https://doi.org/10.1038/sj.mp.4001508

Grothe, M.J., Barthel, H., Sepulcre, J., Dyrba, M., Sabri, O., Teipel, S.J., 2017. In vivo staging of regional amyloid deposition. Neurology 89, 2031–2038. https://doi.org/10.1212/WNL.0000000000004643

Grothe, M.J., Sepulcre, J., Gonzalez-Escamilla, G., Jelistratova, I., Schöll, M., Hansson, O., Teipel, S.J., 2018. Molecular properties underlying regional vulnerability to Alzheimer's disease pathology. Brain 141, 2755–2771. https://doi.org/10.1093/brain/awy189

Guo, T., Brendel, M., Grimmer, T., Rominger, A., Yakushev, I., 2017. Predicting regional pattern of longitudinal β-amyloid accumulation by baseline PET. J. Nucl. Med. 58, 639–645. https://doi.org/10.2967/jnumed.116.176115

Guo, T., Dukart, J., Brendel, M., Rominger, A., Grimmer, T., Yakushev, I., 2018. Rate of β-amyloid accumulation varies with baseline amyloid burden: Implications for anti-amyloid drug trials. Alzheimers Dement. 14, 1387–1396. https://doi.org/10.1016/j.jalz.2018.05.013

Haass, C., Selkoe, D., 2022. If amyloid drives Alzheimer disease, why have anti-amyloid therapies not yet slowed cognitive decline? PLOS Biol. 20, e3001694. https://doi.org/10.1371/journal.pbio.3001694

Haass, C., Selkoe, D.J., 2007. Soluble protein oligomers in neurodegeneration: lessons from the Alzheimer's amyloid β-peptide. Nat. Rev. Mol. Cell Biol. 8, 101–112. https://doi.org/10.1038/nrm2101

Haddad, H.W., Malone, G.W., Comardelle, N.J., Degueure, A.E., Kaye, A.M., Kaye, A.D., 2022. Aducanumab, a Novel Anti-Amyloid Monoclonal Antibody, for the Treatment of

Alzheimer's Disease: A Comprehensive Review. Health Psychol. Res. 10. https://doi.org/10.52965/001c.31925
Hammond, T.C., Xing, X., Wang, C., Ma, D., Nho, K., Crane, P.K., Elahi, F., Ziegler, D.A., Liang, G., Cheng, Q., Yanckello, L.M., Jacobs, N., Lin, A.L., 2020. β-amyloid and tau drive early Alzheimer's disease decline while glucose hypometabolism drives late decline. Commun. Biol. 3, 1–13. https://doi.org/10.1038/s42003-020-1079-x
Harrison, T.M., La Joie, R., Maass, A., Baker, S.L., Swinnerton, K., Fenton, L., Mellinger, T.J., Edwards, L., Pham, J., Miller, B.L., Rabinovici, G.D., Jagust, W.J., 2019. Longitudinal tau accumulation and atrophy in aging and alzheimer disease: Tau-PET and Atrophy. Ann. Neurol. 85, 229–240. https://doi.org/10.1002/ana.25406
He, Z., Guo, J.L., McBride, J.D., Narasimhan, S., Kim, H., Changolkar, L., Zhang, B., Gathagan, R.J., Yue, C., Dengler, C., Stieber, A., Nitla, M., Coulter, D.A., Abel, T., Brunden, K.R., Trojanowski, J.Q., Lee, V.M.Y., 2018. Amyloid-β plaques enhance Alzheimer's brain tau-seeded pathologies by facilitating neuritic plaque tau aggregation. Nat. Med. 24, 29–38. https://doi.org/10.1038/nm.4443
Iglesias, J.E., Van Leemput, K., Bhatt, P., Casillas, C., Dutt, S., Schuff, N., Truran-Sacrey, D., Boxer, A., Fischl, B., 2015. Bayesian segmentation of brainstem structures in MRI. NeuroImage 113, 184–195. https://doi.org/10.1016/j.neuroimage.2015.02.065
Insel, P.S., Mormino, E.C., Aisen, P.S., Thompson, W.K., Donohue, M.C., 2020. Neuroanatomical spread of amyloid β and tau in Alzheimer's disease: implications for primary prevention. Brain Commun. 2, 1–11. https://doi.org/10.1093/braincomms/fcaa007
Ittner, L.M., Götz, J., 2011. Amyloid-β and tau — a toxic pas de deux in Alzheimer´s disease. Nat. Rev. Neurosci. 12, 67–72.
Jack, C.R., Bennett, D.A., Blennow, K., Carrillo, M.C., Dunn, B., Haeberlein, S.B., Holtzman, D.M., Jagust, W., Jessen, F., Karlawish, J., Liu, E., Molinuevo, J.L., Montine, T., Phelps, C., Rankin, K.P., Rowe, C.C., Scheltens, P., Siemers, E., Snyder, H.M., Sperling, R., Elliott, C., Masliah, E., Ryan, L., Silverberg, N., 2018. NIA-AA Research Framework: Toward a biological definition of Alzheimer's disease. Alzheimers Dement. 14, 535–562. https://doi.org/10.1016/j.jalz.2018.02.018
Jack, C.R., Knopman, D.S., Jagust, W.J., Petersen, R.C., Weiner, M.W., Aisen, P.S., Shaw, L.M., Vemuri, P., Wiste, H.J., Weigand, S.D., Lesnick, T.G., Pankratz, V.S., Donohue, M.C., Trojanowski, J.Q., 2013a. Tracking pathophysiological processes in Alzheimer's disease: An updated hypothetical model of dynamic biomarkers. Lancet Neurol. 12, 207–216. https://doi.org/10.1016/S1474-4422(12)70291-0
Jack, C.R., Lowe, V.J., Senjem, M.L., Weigand, S.D., Kemp, B.J., Shiung, M.M., Knopman, D.S., Boeve, B.F., Klunk, W.E., Mathis, C.A., Petersen, R.C., 2008. 11C PiB and structural MRI provide complementary information in imaging of Alzheimer's disease and amnestic mild cognitive impairment. Brain 131, 665–680. https://doi.org/10.1093/brain/awm336
Jack, C.R., Wiste, H.J., Lesnick, T.G., Weigand, S.D., Knopman, D.S., Vemuri, P., Pankratz, V.S., Senjem, M.L., Gunter, J.L., Mielke, M.M., Lowe, V.J., Boeve, B.F., Petersen, R.C., 2013b. Brain β-amyloid load approaches a plateau. Neurology 80, 890–896. https://doi.org/10.1212/WNL.0b013e3182840bbe
Jack, C.R., Wiste, H.J., Weigand, S.D., Knopman, D.S., Mielke, M.M., Vemuri, P., Lowe, V., Senjem, M.L., Gunter, J.L., Reyes, D., Machulda, M.M., Roberts, R., Petersen, R.C.,

2015. Different definitions of neurodegeneration produce similar amyloid/neurodegeneration biomarker group findings. Brain 138, 3747–3759. https://doi.org/10.1093/brain/awv283

Jack, C.R., Wiste, H.J., Weigand, S.D., Therneau, T.M., Lowe, V.J., Knopman, D.S., Gunter, J.L., Senjem, M.L., Jones, D.T., Kantarci, K., Machulda, M.M., Mielke, M.M., Roberts, R.O., Vemuri, P., Reyes, D.A., Petersen, R.C., 2017. Defining imaging biomarker cut points for brain aging and Alzheimer's disease. Alzheimers Dement. 13, 205–216. https://doi.org/10.1016/j.jalz.2016.08.005

Jagust, W., Reed, B., Mungas, D., Ellis, W., DeCarli, C., 2007. What does fluorodeoxyglucose PET imaging add to a clinical diagnosis of dementia? Neurology 69, 871–877. https://doi.org/10.1212/01.wnl.0000269790.05105.16

Jagust, W.J., Landau, S.M., 2021. Temporal Dynamics of Beta-amyloid Accumulation in Aging and Alzheimer's Disease. Neurology 10.1212/WNL.0000000000011524. https://doi.org/10.1212/WNL.0000000000011524

Jelistratova, I., Teipel, S.J., Grothe, M.J., 2020. Longitudinal validity of PET-based staging of regional amyloid deposition. Hum. Brain Mapp. 1–13. https://doi.org/10.1002/hbm.25121

Johnson, K.A., Schultz, A., Betensky, R.A., Becker, J.A., Sepulcre, J., Rentz, D., Mormino, E., Chhatwal, J., Amariglio, R., Papp, K., Marshall, G., Albers, M., Mauro, S., Pepin, L., Alverio, J., Judge, K., Philiossaint, M., Shoup, T., Yokell, D., Dickerson, B., Gomez-Isla, T., Hyman, B., Vasdev, N., Sperling, R., 2016. Tau positron emission tomographic imaging in aging and early Alzheimer disease. Ann. Neurol. 79, 110–119. https://doi.org/10.1002/ana.24546

Joseph-Mathurin, N., Su, Y., Blazey, T.M., Jasielec, M., Vlassenko, A., Friedrichsen, K., Gordon, B.A., Hornbeck, R.C., Cash, L., Ances, B.M., Veale, T., Cash, D.M., Brickman, A.M., Buckles, V., Cairns, N.J., Cruchaga, C., Goate, A., Jack, C.R., Karch, C., Klunk, W., Koeppe, R.A., Marcus, D.S., Mayeux, R., McDade, E., Noble, J.M., Ringman, J., Saykin, A.J., Thompson, P.M., Xiong, C., Morris, J.C., Bateman, R.J., Benzinger, T.L.S., 2018. Utility of perfusion PET measures to assess neuronal injury in Alzheimer's disease. Alzheimers Dement. Diagn. Assess. Dis. Monit. 10, 669–677. https://doi.org/10.1016/j.dadm.2018.08.012

Kadir, A., Almkvist, O., Forsberg, A., Wall, A., Engler, H., Långström, B., Nordberg, A., 2012. Dynamic changes in PET amyloid and FDG imaging at different stages of Alzheimer's disease. Neurobiol. Aging 33, 198.e1-198.e14. https://doi.org/10.1016/j.neurobiolaging.2010.06.015

Khosravi, M., Peter, J., Wintering, N.A., Serruya, M., Shamchi, S.P., Werner, T.J., Alavi, A., Newberg, A.B., 2019. 18F-FDG Is a Superior Indicator of Cognitive Performance Compared to 18F-Florbetapir in Alzheimer's Disease and Mild Cognitive Impairment Evaluation: A Global Quantitative Analysis. J. Alzheimers Dis. 70, 1197–1207. https://doi.org/10.3233/JAD-190220

Kim, J., Basak, J.M., Holtzman, D.M., 2009. The Role of Apolipoprotein E in Alzheimer's Disease. Neuron 63, 287–303. https://doi.org/10.1016/j.neuron.2009.06.026

Klunk, W.E., Engler, H., Nordberg, A., Wang, Y., Blomqvist, G., Holt, D.P., Bergstro, M., Savitcheva, I., Debnath, M.L., Barletta, J., Price, J.C., Sandell, J., Lopresti, B.J., Wall, A., Koivisto, P., Antoni, G., Mathis, C.A., Långstro, B., 2004. Imaging Brain Amyloid in Alzheimer's Disease with Pittsburgh Compound-B. Ann. Neurol. 55, 306–319.

Klunk, W.E., Koeppe, R.A., Price, J.C., Benzinger, T.L., Devous, M.D., Jagust, W.J., Johnson, K.A., Mathis, C.A., Minhas, D., Pontecorvo, M.J., Rowe, C.C., Skovronsky, D.M., Mintun, M.A., 2015. The Centiloid project: Standardizing quantitative amyloid plaque estimation by PET. Alzheimers Dement. 11, 1-15.e4. https://doi.org/10.1016/j.jalz.2014.07.003

Kuschinsky, W., 1991. Coupling of function, metabolism, and blood flow in the brain. Neurosurg. Rev. 14, 163–168. https://doi.org/10.1007/BF00310651

La Joie, R., Visani, A.V., Lesman-Segev, O.H., Baker, S.L., Edwards, L., Iaccarino, L., Soleimani-Meigooni, D.N., Mellinger, T., Janabi, M., Miller, Z.A., Perry, D.C., Pham, J., Strom, A., Gorno-Tempini, M.L., Rosen, H.J., Miller, B.L., Jagust, W.J., Rabinovici, G.D., 2021. Association of *APOE4* and Clinical Variability in Alzheimer Disease With the Pattern of Tau- and Amyloid-PET. Neurology 96, e650–e661. https://doi.org/10.1212/WNL.0000000000011270

Lagarde, J., Olivieri, P., Tonietto, M., Tissot, C., Rivals, I., Gervais, P., Caillé, F., Moussion, M., Bottlaender, M., Sarazin, M., 2022. Tau-PET imaging predicts cognitive decline and brain atrophy progression in early Alzheimer's disease. J. Neurol. Neurosurg. Psychiatry 93, 459–467. https://doi.org/10.1136/jnnp-2021-328623

Lammertsma, A.A., Hume, S.P., 1996. Simplified reference tissue model for PET receptor studies. NeuroImage 4, 153–158. https://doi.org/10.1006/nimg.1996.0066

Landau, S.M., Harvey, D., Madison, C.M., Koeppe, R.A., Reiman, E.M., Foster, N.L., Weiner, M.W., Jagust, W.J., 2011. Associations between cognitive, functional, and FDG-PET measures of decline in AD and MCI. Neurobiol. Aging 32, 1207–1218. https://doi.org/10.1016/j.neurobiolaging.2009.07.002

Landau, S.M., Mintun, M.A., Joshi, A.D., Koeppe, R.A., Petersen, R.C., Aisen, P.S., Weiner, M.W., Jagust, W.J., 2012. Amyloid deposition, hypometabolism, and longitudinal cognitive decline. Ann. Neurol. 72, 578–586. https://doi.org/10.1002/ana.23650

LaPoint, M.R., Chhatwal, J.P., Sepulcre, J., Johnson, K.A., Sperling, R.A., Schultz, A.P., 2017. The association between tau PET and retrospective cortical thinning in clinically normal elderly. NeuroImage 157. https://doi.org/10.1016/j.neuroimage.2017.05.049

Leal, S.L., Lockhart, S.N., Maass, A., Bell, R.K., Jagust, W.J., 2018. Subthreshold Amyloid Predicts Tau Deposition in Aging. J. Neurosci. 38, 4482–4489. https://doi.org/10.1523/JNEUROSCI.0485-18.2018

Leijenaar, J.F., Maurik, I.S., Kuijer, J.P.A., Flier, W.M., Scheltens, P., Barkhof, F., Prins, N.D., 2017. Lower cerebral blood flow in subjects with Alzheimer's dementia, mild cognitive impairment, and subjective cognitive decline using two-dimensional phase-contrast magnetic resonance imaging. Alzheimers Dement. Diagn. Assess. Dis. Monit. 9, 76–83. https://doi.org/10.1016/j.dadm.2017.10.001

Lesman-Segev, O.H., La Joie, R., Iaccarino, L., Lobach, I., Rosen, H.J., Seo, S.W., Janabi, M., Baker, S.L., Edwards, L., Pham, J., Olichney, J., Boxer, A., Huang, E., Gorno-Tempini, M., DeCarli, C., Hepker, M., Hwang, J.L., Miller, B.L., Spina, S., Grinberg, L.T., Seeley, W.W., Jagust, W.J., Rabinovici, G.D., 2021. Diagnostic Accuracy of Amyloid versus ^{18}F-Fluorodeoxyglucose Positron Emission Tomography in AUTOPSY-CONFIRMED Dementia. Ann. Neurol. 89, 389–401. https://doi.org/10.1002/ana.25968

Lim, Y.Y., Mormino, E.C., 2017. APOE genotype and early β-amyloid accumulation in older adults without dementia. Neurology 89, 1028–1034. https://doi.org/10.1212/WNL.0000000000004336

Lockhart, S.N., Schöll, M., Baker, S.L., Ayakta, N., Swinnerton, K.N., Bell, R.K., Mellinger, T.J., Shah, V.D., O'Neil, J.P., Janabi, M., Jagust, W.J., 2017. Amyloid and tau PET demonstrate region-specific associations in normal older people. NeuroImage 150, 191–199. https://doi.org/10.1016/j.neuroimage.2017.02.051

Logan, J., Fowler, J.S., Volkow, N.D., Wang, G.-J., Ding, Y.-S., Alexoff, D.L., 1996. Distribution Volume Ratios Without Blood Sampling from Graphical Analysis of PET Data. J. Cereb. Blood Flow Metab. 16, 834–840.

Lopresti, B.J., Campbell, E.M., Yu, Z., Anderson, S.J., Cohen, A.D., Minhas, D.S., Snitz, B.E., Royse, S.K., Becker, C.R., Aizenstein, H.J., Mathis, C.A., Lopez, O.L., Klunk, W.E., Tudorascu, D.L., 2020. Influence of apolipoprotein-E genotype on brain amyloid load and longitudinal trajectories. Neurobiol. Aging 94, 111–120. https://doi.org/10.1016/j.neurobiolaging.2020.05.012

Mathis, C.A., Wang, Y., Holt, D.P., Huang, G.F., Debnath, M.L., Klunk, W.E., 2003. Synthesis and evaluation of 11C-labeled 6-substituted 2-arylbenzothiazoles as amyloid imaging agents. J. Med. Chem. 46, 2740–2754. https://doi.org/10.1021/jm030026b

Mattsson, N., Palmqvist, S., Stomrud, E., Vogel, J., Hansson, O., 2019. Staging β -Amyloid Pathology With Amyloid Positron Emission Tomography. JAMA Neurol. 76, 1319–1329. https://doi.org/10.1001/jamaneurol.2019.2214

Mattsson, N., Tosun, D., Insel, P.S., Simonson, A., Jr, C.R.J., Beckett, L.A., Donohue, M., Jagust, W., Schuff, N., 2014. Association of brain amyloid- b with cerebral perfusion and structure in Alzheimer ' s disease and mild cognitive impairment. Brain 137, 1550–1561. https://doi.org/10.1093/brain/awu043

McLean, C.A., Cherny, R.A., Fraser, F.W., Fuller, S.J., Smith, M.J., Konrad Vbeyreuther, Bush, A.I., Masters, C.L., 1999. Soluble pool of A? amyloid as a determinant of severity of neurodegeneration in Alzheimer's disease. Ann. Neurol. 46, 860–866. https://doi.org/10.1002/1531-8249(199912)46:6<860::AID-ANA8>3.0.CO;2-M

Meyer, P.T., Hellwig, S., Amtage, F., Rottenburger, C., Sahm, U., Reuland, P., Weber, W.A., Hüll, M., 2011. Dual-biomarker imaging of regional cerebral amyloid load and neuronal activity in dementia with PET and11C-Labeled Pittsburgh compound B. J. Nucl. Med. 52, 393–400. https://doi.org/10.2967/jnumed.110.083683

Michels, L., Warnock, G., Buck, A., Macauda, G., Leh, S.E., Kaelin, A.M., Riese, F., Meyer, R., O'Gorman, R., Hock, C., Kollias, S., Gietl, A.F., 2016. Arterial spin labeling imaging reveals widespread and Aβ-independent reductions in cerebral blood flow in elderly apolipoprotein epsilon-4 carriers. J. Cereb. Blood Flow Metab. 36, 581–595. https://doi.org/10.1177/0271678X15605847

Minoshima, S., Giordani, B., Berent, S., Frey, K.A., Foster, N.L., Kuhl, D.E., 1997. Metabolic reduction in the posterior cingulate cortex in very early Alzheimer's disease. Ann. Neurol. 42, 85–94. https://doi.org/10.1002/ana.410420114

Mishra, S., Blazey, T.M., Holtzman, D.M., Cruchaga, C., Su, Y., Morris, J.C., Benzinger, T.L.S., Gordon, B.A., 2018. Longitudinal brain imaging in preclinical Alzheimer disease: Impact of APOE ϵ4 genotype. Brain 141, 1828–1839. https://doi.org/10.1093/brain/awy103

Mormino, E.C., Betensky, R.A., Hedden, T., Schultz, A.P., Amariglio, R.E., Rentz, D.M., Johnson, K.A., Sperling, R.A., 2014. Synergistic effect of β-amyloid and neurodegeneration on cognitive decline in clinically normal individuals. JAMA Neurol. 71, 1379–1385. https://doi.org/10.1001/jamaneurol.2014.2031

Mormino, E.C., Kluth, J.T., Madison, C.M., Rabinovici, G.D., Baker, S.L., Miller, B.L., Koeppe, R.A., Mathis, C.A., Weiner, M.W., Jagust, W.J., 2009. Episodic memory loss is related to hippocampal-mediated β-amyloid deposition in elderly subjects. Brain 132, 1310–1323. https://doi.org/10.1093/brain/awn320

Mormino, E.C., Smiljic, A., Hayenga, A.O., H. Onami, S., Greicius, M.D., Rabinovici, G.D., Janabi, M., Baker, S.L., V. Yen, I., Madison, C.M., Miller, B.L., Jagust, W.J., 2011. Relationships between beta-amyloid and functional connectivity in different components of the default mode network in aging. Cereb. Cortex 21, 2399–2407. https://doi.org/10.1093/cercor/bhr025

Morris, J.C., 1993. The Clinical Dementia Rating (CDR): current version and scoring rules. Neurology 43, 2412–2414. https://doi.org/10.1212/WNL.43.11.2412-a

Mosconi, L., 2005. Brain glucose metabolism in the early and specific diagnosis of Alzheimer?s disease: FDG-PET studies in MCI and AD. Eur. J. Nucl. Med. Mol. Imaging 32, 486–510. https://doi.org/10.1007/s00259-005-1762-7

Mowinkel, A.M., Vidal-Piñeiro, D., 2019. Visualisation of Brain Statistics with R-packages ggseg and ggseg3d. arXiv 1912.08200.

Müller, U.C., Deller, T., Korte, M., 2017. Not just amyloid: physiological functions of the amyloid precursor protein family. Nat. Rev. Neurosci. 18, 281–298. https://doi.org/10.1038/nrn.2017.29

Näslund, J., Haroutunian, V., Mohs, R., Davis, K.L., Davies, P., Greengard, P., Buxbaum, J.D., 1999. Correlation between elevated levels of amyloid β-peptide in the brain and cognitive decline. JAMA 283, 1571–1577.

Nihashi, T., Yatsuya, H., Hayasaka, K., Kato, R., Kawatsu, S., Arahata, Y., Iwai, K., Takeda, A., Washimi, Y., Yoshimura, K., Mizuno, K., Kato, T., Naganawa, S., Ito, K., 2007. Direct comparison study between FDG-PET and IMP-SPECT for diagnosing Alzheimer's disease using 3D-SSP analysis in the same patients. Radiat. Med. - Med. Imaging Radiat. Oncol. 25, 255–262. https://doi.org/10.1007/s11604-007-0132-8

Noda, A., Ohba, H., Kakiuchi, T., Futatsubashi, M., Tsukada, H., Nishimura, S., 2002. Age-related changes in cerebral blood flow and glucose metabolism in conscious rhesus monkeys. Brain Res. 936, 76–81. https://doi.org/10.1016/S0006-8993(02)02558-1

Nordberg, A., Rinne, J.O., Kadir, A., Lngström, B., 2010. The use of PET in Alzheimer disease. Nat. Rev. Neurol. 6, 78–87. https://doi.org/10.1038/nrneurol.2009.217

Oh, H., Madison, C., Baker, S., Rabinovici, G., Jagust, W., 2016. Dynamic relationships between age, amyloid-β deposition, and glucose metabolism link to the regional vulnerability to Alzheimer's disease. Brain 139, 2275–2289. https://doi.org/10.1093/brain/aww108

Okamura, N., Harada, R., Ishiki, A., Kikuchi, A., Nakamura, T., Kudo, Y., 2018. The development and validation of tau PET tracers: current status and future directions. Clin. Transl. Imaging 6, 305–316. https://doi.org/10.1007/s40336-018-0290-y

Oliveira, F.P.M., Moreira, A.P., Mendonça, A.D., Verdelho, A., Xavier, C., Barroca, D., Rio, J., Cardoso, E., Cruz, Â., Abrunhosa, A., Castelo-Branco, M., 2018. Can 11 C-PiB-PET relative delivery R 1 or 11 C-PiB-PET perfusion replace 18 F-FDG-PET in the assessment of brain neurodegeneration? J. Alzheimers Dis. 65, 89–97. https://doi.org/10.3233/JAD-180274

Ossenkoppele, R., Schonhaut, D.R., Schöll, M., Lockhart, S.N., Ayakta, N., Baker, S.L., O'Neil, J.P., Janabi, M., Lazaris, A., Cantwell, A., Vogel, J., Santos, M., Miller, Z.A., Bettcher, B.M., Vossel, K.A., Kramer, J.H., Gorno-Tempini, M.L., Miller, B.L., Jagust, W.J.,

Rabinovici, G.D., 2016. Tau PET patterns mirror clinical and neuroanatomical variability in Alzheimer's disease. Brain 139, 1551–1567. https://doi.org/10.1093/brain/aww027
Ottoy, J., Verhaeghe, J., Niemantsverdriet, E., Roeck, E.D., wyffels, L., Ceyssens, S., Broeckhoven, C.V., Engelborghs, S., Stroobants, S., Staelens, S., 2019. 18F-FDG PET, the early phases and the delivery rate of 18F-AV45 PET as proxies of cerebral blood flow in Alzheimer's disease: Validation against 15O-H2O PET. Alzheimers Dement. 15, 1172–1182. https://doi.org/10.1016/j.jalz.2019.05.010
Palmqvist, S., Schöll, M., Strandberg, O., Mattsson, N., Stomrud, E., Zetterberg, H., Blennow, K., Landau, S., Jagust, W., Hansson, O., 2017. Earliest accumulation of β-amyloid occurs within the default-mode network and concurrently affects brain connectivity. Nat. Commun. 8. https://doi.org/10.1038/s41467-017-01150-x
Pascoal, T.A., Mathotaarachchi, S., Shin, M., Benedet, A.L., Mohades, S., Wang, S., Beaudry, T., Kang, M.S., Rosa-Neto, P., Benedet, A.L., Soucy, J.P., Labbe, A., Labbe, A., Gauthier, S., Gauthier, S., 2017. Synergistic interaction between amyloid and tau predicts the progression to dementia. Alzheimers Dement. 13, 644–653. https://doi.org/10.1016/j.jalz.2016.11.005
Paulson, O.B., Hasselbalch, S.G., Rostrup, E., Knudsen, G.M., Pelligrino, D., 2010. Cerebral blood flow response to functional activation. J. Cereb. Blood Flow Metab. 30, 2–14. https://doi.org/10.1038/jcbfm.2009.188
Peretti, D.E., García, D.V., Reesink, F.E., Goot, T.V. der, Deyn, P.P.D., Jong, B.M.D., Dierckx, R.A.J.O., Boellaard, R., 2019. Relative cerebral flow from dynamic PIB scans as an alternative for FDG scans in Alzheimer's disease PET studies. PLoS ONE 14, 1–19. https://doi.org/10.1371/journal.pone.0211000
Pooler, A.M., Polydoro, M., Maury, E.A., Nicholls, S.B., Reddy, S.M., Wegmann, S., William, C., Saqran, L., Cagsal-Getkin, O., Pitstick, R., Beier, D.R., Carlson, G.A., Spires-Jones, T.L., Hyman, B.T., 2015. Amyloid accelerates tau propagation and toxicity in a model of early Alzheimer's disease. Acta Neuropathol. Commun. 3, 1–11. https://doi.org/10.1186/s40478-015-0199-x
Price, J.C., Klunk, W.E., Lopresti, B.J., Lu, X., Hoge, J.A., Ziolko, S.K., Holt, D.P., Meltzer, C.C., DeKosky, S.T., Mathis, C.A., 2005. Kinetic modeling of amyloid binding in humans using PET imaging and Pittsburgh Compound-B. J. Cereb. Blood Flow Metab. 25, 1528–1547. https://doi.org/10.1038/sj.jcbfm.9600146
Rabinovici, G.D., Rosen, H.J., Alkalay, A., Kornak, J., Furst, A.J., Agarwal, N., Mormino, E.C., O'Neil, J.P., Janabi, M., Karydas, A., Growdon, M.E., Jang, J.Y., Huang, E.J., DeArmond, S.J., Trojanowski, J.Q., Grinberg, L.T., Gorno-Tempini, M.L., Seeley, W.W., Miller, B.L., Jagust, W.J., 2011. Amyloid vs FDG-PET in the differential diagnosis of AD and FTLD. Neurology 77, 2034–2042. https://doi.org/10.1212/WNL.0b013e31823b9c5e
Rentz, D.M., Locascio, J.J., Becker, J.A., Moran, E.K., Eng, E., Buckner, R.L., Sperling, R.A., Johnson, K.A., 2010. Cognition, reserve and amyloid deposition in normal aging. Ann. Neurol. 353–364. https://doi.org/10.1002/ana.21904
Resnick, S.M., Bilgel, M., Moghekar, A., An, Y., Cai, Q., Wang, M.C., Thambisetty, M., Prince, J.L., Zhou, Y., Soldan, A., Wong, D.F., O'Brien, R.J., Ferrucci, L., Albert, M.S., 2015. Changes in Aβ biomarkers and associations with APOE genotype in 2 longitudinal cohorts. Neurobiol. Aging 36, 2333–2339. https://doi.org/10.1016/j.neurobiolaging.2015.04.001

Rocher, A.B., Chapon, F., Blaizot, X., Baron, J.-C., Chavoix, C., 2003. Resting-state brain glucose utilization as measured by PET is directly related to regional synaptophysin levels: a study in baboons. NeuroImage 20, 1894–1898. https://doi.org/10.1016/j.neuroimage.2003.07.002

Rodriguez-Vieitez, E., Leuzy, A., Chiotis, K., Saint-Aubert, L., Wall, A., Nordberg, A., 2017. Comparability of [18F]THK5317 and [11C]PIB blood flow proxy images with [18F]FDG positron emission tomography in Alzheimer's disease. J. Cereb. Blood Flow Metab. 37, 740–749. https://doi.org/10.1177/0271678X16645593

Rostomian, A.H., Madison, C., Rabinovici, G.D., Jagust, W.J., 2011. Early 11C-PIB frames and 18F-FDG PET measures are comparable: A study validated in a cohort of AD and FTLD patients. J. Nucl. Med. 52, 173–179. https://doi.org/10.2967/jnumed.110.082057

Rousset, O.G., Ma, Y., Evans, A.C., 1998. Correction for partial volume effects in PET : principle and validation . J Correction for Partial Volume Effects in PET : Principle and Validation. J. Nucl. Med. 39, 904–911.

Sakono, M., Zako, T., 2010. Amyloid oligomers: Formation and toxicity of Aβ oligomers. FEBS J. 277, 1348–1358. https://doi.org/10.1111/j.1742-4658.2010.07568.x

Salahuddin, P., Fatima, M.T., Abdelhameed, A.S., Nusrat, S., Khan, R.H., 2016. Structure of amyloid oligomers and their mechanisms of toxicities: Targeting amyloid oligomers using novel therapeutic approaches. Eur. J. Med. Chem. 114, 41–58. https://doi.org/10.1016/j.ejmech.2016.02.065

Scheffer, S., Hermkens, D.M.A., van der Weerd, L., de Vries, H.E., Daemen, M.J.A.P., 2021. Vascular Hypothesis of Alzheimer Disease: Topical Review of Mouse Models. Arterioscler. Thromb. Vasc. Biol. 41, 1265–1283. https://doi.org/10.1161/ATVBAHA.120.311911

Schöll, M., Lockhart, S.N., Schonhaut, D.R., O'Neil, J.P., Janabi, M., Ossenkoppele, R., Baker, S.L., Vogel, J.W., Faria, J., Schwimmer, H.D., Rabinovici, G.D., Jagust, W.J., 2016. PET Imaging of Tau Deposition in the Aging Human Brain. Neuron 89, 971–982. https://doi.org/10.1016/j.neuron.2016.01.028

Shankar, G.M., Li, S., Mehta, T.H., Garcia-Munoz, A., Shepardson, N.E., Smith, I., Brett, F.M., Farrell, M.A., Rowan, M.J., Lemere, C.A., Regan, C.M., Walsh, D.M., Sabatini, B.L., Selkoe, D.J., 2008. Amyloid-β protein dimers isolated directly from Alzheimer's brains impair synaptic plasticity and memory. Nat. Med. 14, 837–842. https://doi.org/10.1038/nm1782

Silverman, D.H.S., Small, G.W., Chang, C.Y., Lu, C.S., de Aburto, M.A.K., Chen, W., Czernin, J., Rapoport, S.I., Pietrini, P., Alexander, G.E., Schapiro, M.B., Jagust, W.J., Hoffman, J.M., Welsh-Bohmer, K.A., Alavi, A., Clark, C.M., Salmon, E., de Leon, M.J., Mielke, R., Cummings, J.L., Kowell, A.P., Gambhir, S.S., Hoh, C.K., Phelps, M.E., 2001. Positron Emission Tomography in Evaluation of Dementia: Regional Brain Metabolism and Long-term Outcome. JAMA 286, 2120. https://doi.org/10.1001/jama.286.17.2120

Sojkova, J., Beason-Held, L., Zhou, Y., An, Y., Kraut, M.A., Ye, W., Ferrucci, L., Mathis, C.A., Klunk, W.E., Wong, D.F., Resnick, S.M., 2008. Longitudinal Cerebral Blood Flow and Amyloid Deposition: An Emerging Pattern? J. Nucl. Med. 49, 1465–1471. https://doi.org/10.2967/jnumed.108.051946

Sperling, R.A., Aisen, P.S., Beckett, L.A., Bennett, D.A., Craft, S., Fagan, A.M., Iwatsubo, T., Jack, C.R., Kaye, J., Montine, T.J., Park, D.C., Reiman, E.M., Rowe, C.C., Siemers, E., Stern, Y., Yaffe, K., Carrillo, M.C., Thies, B., Morrison-bogorad, M., Wagster, M.V.,

Phelps, C.H., 2011. Toward defining the preclinical stages of Alzheimer's disease : Recommendations from the National Institute on Aging-Alzheimer ' s Association workgroups on diagnostic guidelines for Alzheimer ' s disease. Alzheimers Dement. 7, 280–292. https://doi.org/10.1016/j.jalz.2011.03.003

Strom, A., Iaccarino, L., Edwards, L., Lesman-Segev, O.H., Soleimani-Meigooni, D.N., Pham, J., Baker, S.L., Landau, S.M., Jagust, W.J., Miller, B.L., Rosen, H.J., Gorno-Tempini, M.L., Rabinovici, G.D., La Joie, R., for the Alzheimer's Disease Neuroimaging Initiative, 2022. Cortical hypometabolism reflects local atrophy and tau pathology in symptomatic Alzheimer's disease. Brain 145, 713–728. https://doi.org/10.1093/brain/awab294

Teipel, S.J., Dyrba, M., Chiesa, P.A., Sakr, F., Jelistratova, I., Lista, S., Vergallo, A., Lemercier, P., Cavedo, E., Habert, M.O., Dubois, B., Hampel, H., Grothe, M.J., 2020. In vivo staging of regional amyloid deposition predicts functional conversion in the preclinical and prodromal phases of Alzheimer's disease. Neurobiol. Aging 93, 98–108. https://doi.org/10.1016/j.neurobiolaging.2020.03.011

Teng, E., Manser, P.T., Sanabria Bohorquez, S., Wildsmith, K.R., Pickthorn, K., Baker, S.L., Ward, M., Kerchner, G.A., Weimer, R.M., 2021. Baseline [18F]GTP1 tau PET imaging is associated with subsequent cognitive decline in Alzheimer's disease. Alzheimers Res. Ther. 13, 196. https://doi.org/10.1186/s13195-021-00937-x

Thal, D.R., Rüb, U., Orantes, M., Braak, H., 2002. Phases of Aβ-deposition in the human brain and its relevance for the development of AD. Neurology 58, 1791–1800.

Thinakaran, G., Koo, E.H., 2008. Amyloid Precursor Protein Trafficking, Processing, and Function. J. Biol. Chem. 283, 29615–29619. https://doi.org/10.1074/jbc.R800019200

Tosun, D., Landau, S., Aisen, P.S., Petersen, R.C., Mintun, M., Jagust, W., Weiner, M.W., 2017. Association between tau deposition and antecedent amyloid-β accumulation rates in normal and early symptomatic individuals. Brain 140, 1499–1512. https://doi.org/10.1093/brain/awx046

van der Kall, L.M., Truong, T., Burnham, S.C., Doré, V., Mulligan, R.S., Bozinovski, S., Lamb, F., Bourgeat, P., Fripp, J., Schultz, S., Lim, Y.Y., Laws, S.M., Ames, D., Fowler, C., Rainey-Smith, S.R., Martins, R.N., Salvado, O., Robertson, J., Maruff, P., Masters, C.L., Villemagne, V.L., Rowe, C.C., 2021. Association of β-amyloid level, clinical progression and longitudinal cognitive change in normal older individuals. Neurology 96, e662–e6670. https://doi.org/10.1212/WNL.0000000000011222

Vemuri, P., Lowe, V.J., Knopman, D.S., Senjem, M.L., Kemp, B.J., Schwarz, C.G., Przybelski, S.A., Machulda, M.M., Petersen, R.C., Jack, C.R., 2017. Tau-PET uptake : Regional variation in average SUVR and impact of amyloid deposition. Alzheimers Dement. Diagn. Assess. Dis. Monit. 6, 21–30. https://doi.org/10.1016/j.dadm.2016.12.010

Villemagne, V.L., Burnham, S., Bourgeat, P., Brown, B., Ellis, K.A., Salvado, O., Szoeke, C., Macaulay, S.L., Martins, R., Maruff, P., Ames, D., Rowe, C.C., Masters, C.L., 2013. Amyloid β deposition, neurodegeneration, and cognitive decline in sporadic Alzheimer's disease: A prospective cohort study. Lancet Neurol. 12, 357–367. https://doi.org/10.1016/S1474-4422(13)70044-9

Villeneuve, S., Rabinovici, G.D., Cohn-Sheehy, B.I., Madison, C., Ayakta, N., Ghosh, P.M., Joie, R.L., Arthur-bentil, S.K., Vogel, J.W., Marks, S.M., Lehmann, M., Rosen, H.J., Reed, B., Olichney, J., Boxer, A.L., Miller, B.L., Borys, E., Jin, L., Huang, E.J., Grinberg, L.T., Decarli, C., Seeley, W.W., Jagust, W., 2015. Existing Pittsburgh

Compound-B positron emission tomography thresholds are too high: statistical and pathological evaluation. Brain 138, 2020–2033. https://doi.org/10.1093/brain/awv112
Visser, D., Wolters, E.E., Verfaillie, S.C.J., Coomans, E.M., Timmers, T., Tuncel, H., Reimand, J., Boellaard, R., Windhorst, A.D., Scheltens, P., van der Flier, W.M., Ossenkoppele, R., van Berckel, B.N.M., 2020. Tau pathology and relative cerebral blood flow are independently associated with cognition in Alzheimer's disease. Eur. J. Nucl. Med. Mol. Imaging 47, 3165–3175. https://doi.org/10.1007/s00259-020-04831-w
Vlassenko, A.G., Vaishnavi, S.N., Couture, L., Sacco, D., Shannon, B.J., Mach, R.H., Morris, J.C., Raichle, M.E., Mintun, M.A., 2010. Spatial correlation between brain aerobic glycolysis and amyloid-β (Aβ) deposition. Proc. Natl. Acad. Sci. U. S. A. 107, 17763–17767. https://doi.org/10.1073/pnas.1010461107
Vogel, J.W., Iturria-Medina, Y., Strandberg, O.T., Smith, R., Levitis, E., Evans, A.C., Hansson, O., 2020. Spread of pathological tau proteins through communicating neurons in human Alzheimer's disease. Nat. Commun. 11, 2612. https://doi.org/10.1038/s41467-020-15701-2
Whittington, A., Sharp, D.J., Gunn, R.N., 2018. Spatiotemporal distribution of B-Amyloid in Alzheimer disease is the result of heterogeneous regional carrying capacities. J. Nucl. Med. 59, 822–827. https://doi.org/10.2967/jnumed.117.194720
Wu, Y., Carson, R.E., 2002. Noise reduction in the simplified reference tissue model for neuroreceptor functional imaging. J. Cereb. Blood Flow Metab. 22, 1440–1452. https://doi.org/10.1097/01.WCB.0000033967.83623.34
Yotter, R.A., Doshi, J., Clark, V., Sojkova, J., Zhou, Y., Wong, D.F., Ferrucci, L., Resnick, S.M., Davatzikos, C., 2013. Memory decline shows stronger associations with estimated spatial patterns of amyloid deposition progression than total amyloid burden. Neurobiol. Aging 34, 2835–2842. https://doi.org/10.1016/j.neurobiolaging.2013.05.030.Memory
Youden, W.J., 1950. Index for rating diagnostic tests. Cancer 3, 32–35. https://doi.org/10.1002/1097-0142(1950)3:1<32::AID-CNCR2820030106>3.0.CO;2-3
Zimmer, E.R., Parent, M.J., Souza, D.G., Leuzy, A., Lecrux, C., Kim, H.-I., Gauthier, S., Pellerin, L., Hamel, E., Rosa-Neto, P., 2017. [18F]FDG PET signal is driven by astroglial glutamate transport. Nat. Neurosci. 20, 393–395. https://doi.org/10.1038/nn.4492